IN THE NAME OF ALLAH,
THE MOST GRACIOUS,
THE MOST MERCIFUL

Kingdom of Saudi Arabia
Ministry of Education
Majmaah University

جامعة المجمعة
Majmaah University

JEAS

JOURNAL OF ENGINEERING AND APPLIED SCIENCES

A Refereed Academic Journal Published by the
Publishing and Translation Center at Majmaah Universtiy

Vol. 3, Issue (1) May, 2016 ISSN: 1658 - 6638

Publishing & Translation Center - MU

About the Journal

Journal of Engineering and Applied Sciences (JEAS)

Vision

Pioneer journal in the publication of advanced research in engineering and applied sciences.

Mission

A peer-review process which is transparent and rigorous

Objectives

a) Support research that addresses current problems facing humanity.
b) Provide an avenue for exchange of research interests and facilitate the communication among researchers.

Scope

JEAS accepts articles in the field of engineering and applied sciences. Engineering areas covered by JEAS include:

Engineering areas

Architectural Engineering
Chemical Engineering
Civil Engineering
Computer Engineering
Electrical Engineering
Environmental Engineering
Industrial Engineering
Mechanical Engineering

Applied Sciences areas

Applied Mathematics
Applied Physics
Biological Science
Biomathematics
Biotechnology
Computer Sciences
Earth Science
Environmental Science

Correspondence and Subscription

Majmaah University, Post Box 66, AlMajmaah 11952, KSA

email: jeas@mu.edu.sa

Journal of Engineering and Applied Sciences

Editorial

Scientific publishing has brought many challenges to authors. With increasing number of scientific journals, varying scopes and reviewing requirements, and cost of publishing to authors, finding the right journal to publish an article is a decision many authors must bitterly confront and resolve. The publication of scientific findings is an integral part of the life of researchers; and the process of publishing has evolved to become an efficient system of decimating knowledge and collaboration among scientists. Science journals have institutionalized procedures to manage large volume of article submissions per year; in many cases, journals began to define narrower scopes for a dual purpose: managing submissions and delivering outstanding research.

Based on recent studies, the scientific publishing world consists of more than 25 thousands active journals in various disciplines and fields. Science Direct hosts 3,348 journals (as of February 2014). The Directory of Open Access Journals lists in its search engine more than 9,800 open access online journals.

According to recent estimates, the number of scientific journals grows by 3% per year worldwide. With this large number of journals, journals may find it harder to stay afloat.

In its inauguration, the board of editors is honored to introduce to the scientific community the Journal of Engineering and Applied Sciences - JEAS, another scientific journal from Majmaah University. The board has pledged a commitment to JEAS authors and readers to bring the most dynamic and vibrant journal management with better satisfaction.

Dr. Sameh S. Ahmed

Contents

Effect of Radiation and Double Dispersion on Mixed Convection Heat and Mass Transfer in Non-Darcy Porous Medium

M. A. El-Hakiem
Department of Mathematics , College of Science, Majmaah University, Al-Zulfi, Kingdom of Saudi Arabia,

Abdullah Abduljabar Ansari
Department of Mathematics , College of Science, Majmaah University, Al-Zulfi, Kingdom of Saudi Arabia,
a.ansari@mu.edu.sa

Abstract

Similarity solution for the problem of hydrodynamic dispersion and radiation in non- Darcy mixed convection heat and mass transfer from vertical surface embedded in porous media is presented. The Forchheimer extension is considered in the governing equations. The heat and mass transfer in the boundary layer region for aiding and opposing buoyancies in both flows has been analyzed. The Rosseland approximation is used to describe the radiative heat flux in the energy equation. The dimensionless velocity, temperature and concentration fields in the non-Darcy porous media are governed by complex interactions among the diffusion rate, buoyancy ratio and radiation parameter in addition to the flow driving parameter. Numerical results for details of the dimensionless velocity, temperature and concentration which shown on graphs and tables have been presented and compared against previously published work on special cases of the problem and found to be in excellent agreement. The combined effects of radiation, thermal dispersion and solutal diffusivity, for the non-Darcy porous medium, on the dimensionless velocity and heat and mass coefficients are discussed.

Keywords: Radiation ; Mixed Convection; Double Dispersion ; Porous Medium; Non-Darcy; Boundary Layer ; Heat and Mass Transfer

1. Introduction

Thermal and solutal transport by fluid flowing through a porous matrix is a phenomenon of great interest from both the theory and application point of view. The flow phenomenon is relatively complex rather than that of the pure thermal convection process. Heat and mass transfer processes in porous media are often encountered in the study of dynamics hot and salty springs of a sea, and in the chemical industry, in reservoir engineering about thermal recovery process. and other pollutants, grain storage, evaporation cooling, and solidification are the few other application areas where the combined thermo-solutal mixed convection in porous media are observed.

Combined heat and mass transfer by free convection under boundary layer approximations has been studied by Bejan and Khair [1] and Murthy and Singh [2]. Mixed convection boundary layer flow on a

surface in a saturated porous medium was studied by Merkin [3]. Coupled heat and mass transfer by mixed convection in Darcian fluid-saturated porous medium has been analyzed by Lai [4]. Thermal dispersion effects have been studied by Lai and Kulacki [5], Amiri and Vafai [6] and Murthy and Singh [7]. Coupled heat and mass transfer phenomenon in non-Darcy flows are studied by Karimi-Fard et al. [8] and Murthy and Singh [2]. The effect of solutal and thermal dispersion effects in homogeneous and isotropic Darcian porous media has been analyzed by Dagan [9]. A systematic derivation of the governing equations with various types of approximations used in applications has been presented. Using scale analysis arguments, Telles, and Trevisan [10] analyzed the double dispersion phenomenon in a free convection boundary layer adjacent to a vertical wall in a Darcian fluid-saturated porous medium. Murthy and Singh [11] studied the convective heat transfer in non-Darcy porous media. The effect of double dispersion on mixed convection heat and mass transfer in non-Darcy porous medium has been analyzed under boundary layer approximations using the similarity solution technique by Murthy [12]. Mansour and El-Amin [13] studied the thermal dispersion effects on non-Darcy axisymmetric free convection in a saturated porous medium. Double dispersion effects on natural convection heat and mass transfer in non-Darcy porous medium studied by El-Amin [14].

and Takhar [15] studied the effects of thermal radiation on mixed convection along a vertical plate subjected to uniform surface temperature. The problem of steady two-dimensional free convection flow through a very porous medium bounded by a vertical infinite porous plate by the presence of thermal radiation was considered by Raptis [16]. The problem of thermal dispersion-radiation effects on non-Darcy natural convection in a fluid saturated porous medium studied by Mohammadien and El-Amin [17]. Thermal radiation effect on non-Darcy natural convection with lateral mass transfer investigated by El-Hakiem and El-Amin [18]. El-Hakiem [19] studied radiative effects on non-Darcy natural convection from a heated vertical plate in saturated porous media with mass transfer for non-Newtonian fluid. Heat and mass transfer by non-Darcy free convection from a vertical cylinder embedded in porous media with a temperature dependent viscosity investigated by Chamkha, et al. [20]. Effect of rotation on thermal convection in an anisotropic porous medium with temperature dependent viscosity was studied by Vanishree [21]. El-Hakiem et al. [22] studied Natural convection boundary layer of non-Newtonian fluid about a permeable vertical Cone embedded in porous medium saturated with a nanofluid. Chamkha, A.J., et.al. [23] studied Coupled heat and mass transfer by MHD free convection flow along a vertical plate with streamwise temperature and species concentration variations. Nield and Bejan [24] explained about convective

heat transfer in porous medium in their book. Kairi and Murthy [25] investigated the effect of double dispersion on mixed convection heat and mass transfer in a non-Newtonian fluid-saturated non-Darcy porous medium. Srinivasacharya, D., et. al. [26] studied mixed convection heat and mass transfer along a vertical plate embedded in a power-law fluid saturated Darcy porous medium with chemical reaction and radiation effects.

The present work, investigates the effects of double dispersion-radiation on mixed convection heat and mass transfer in non-Darcy porous medium. The Forchheimer flow model is considered and the porous medium porosity is assumed to be low so that the boundary effects in the medium may be neglected. The heat and mass transfer in the boundary layer region has analyzed for aiding and opposing buoyancies for both aiding and opposing flows. The dimensionless velocity, temperature and concentration fields in non-Darcy porous media are observed to be governed by complex interactions among the diffusions rate Le, buoyancy ratio N, Pe_γ and Pe_ξ the dispersion thermal and solutal diffusivity parameters respectively and radiation parameter R. The Rosseland approximation is used to describe the radiative heat flux in the energy equation.

2. Analysis

Mixed convection heat and mass transfer from the impermeable vertical flat wall in a fluid-saturated porous medium is considered for the study. The x-axis is taken along the plate and the y-coordinate normal to it. The wall is maintained at constant temperature and concentration, T_w and C_w respectively, and these values are assumed to be greater than the ambient temperature and concentration T_∞ and C_∞ respectively. The gravitational acceleration g is in a direction opposite to x-direction. The radiative heat flux in the x-direction is consider negligible in comparison with that in the y-direction. The governing equations for the boundary layer flow, heat and mass transfer from the wall $y = 0$ into the fluid-saturated porous medium $x \geq 0$ and $y > 0$ (after making use of the Boussinesq approximation).

$$\frac{\partial u}{\partial x} + \frac{\partial v}{\partial y} = 0 \tag{1}$$

$$\frac{\partial u}{\partial y} + \frac{c\sqrt{K}}{\nu}\frac{\partial u^2}{\partial y} = \left(\frac{Kg\beta_T}{\nu}\right)\frac{\partial T}{\partial y} + \left(\frac{Kg\beta_C}{\nu}\right)\frac{\partial C}{\partial y} \quad ,(2)$$

$$u\frac{\partial T}{\partial x} + v\frac{\partial T}{\partial y} = \frac{\partial}{\partial y}\left(\alpha_{ff}\frac{\partial T}{\partial y}\right) - \frac{\alpha}{k}\frac{\partial q^r}{\partial y}, \tag{3}$$

$$u\frac{\partial C}{\partial x} + v\frac{\partial C}{\partial y} = \frac{\partial}{\partial y}(D_C\frac{\partial C}{\partial y}), \tag{4}$$

The boundary conditions are:

$$y = 0: \quad v = 0, \quad T = T_w, \quad C = C_w$$

$$y \to \infty: \quad u = u_\infty, \quad T = T_\infty, \quad C = C_\infty \tag{5}$$

Here x and y are the Cartesian coordinates, u and v are the averaged velocity components in x and y-directions respectively; T is the temperature; C is the concentration; ν is the kinematic viscosity of the fluid; β_T is the coefficient of thermal expansion; β_C is the coefficient of solutal expansion; K the permeability of the porous medium; k the thermal conductivity; c an empirical constant; g the acceleration due to gravity; α the equivalent thermal diffusivity of the porous medium; α_{ff} and D_C are the effective thermal and solutal diffusivities, respectively. Telles and Trevisan (1993) investigate $\alpha_{ff} = \alpha + \gamma du$, $D_C = D + \xi du$, whereas γdu and ξdu represent dispersion thermal and solutal diffusivities, respectively. The quantity q^r represents the radiative heat flux in the y-direction. The radiative heat flux term is simplified by using the Rosseland approximation as:

$$q^r = -\frac{4\sigma}{3k_0}\frac{\partial T^4}{\partial y}, \tag{6}$$

where σ and k_0 are the Stefan-Boltzman constant and the mean absorption coefficient, respectively.

Proceeding with the analysis, we define the following transformations:

$$\eta = (\frac{y}{x})Pe_x^{1/2} \quad , \qquad f(\eta) = \frac{\psi}{\alpha Pe_x^{1/2}} \quad ,$$

$$\theta(\eta) = \frac{(T - T_\infty)}{(T_w - T_\infty)}, \ \phi(\eta) = \frac{(C - C_\infty)}{(C_w - C_\infty)} \tag{7}$$

Substituting the expressions in (7) into equations (2), (3) and (4), the transformed governing equations may be written as:

$$f'' + 2F_0 Peff'' = \pm\frac{Ra}{Pe}[\theta' + N\phi'] \tag{8}$$

$$\theta'' + \frac{1}{2}f\,\theta' + Pe_\gamma[f'\theta'' + f''\theta'] + \frac{4R[(\theta + C_T)^3\theta']'}{3} = 0 \tag{9}$$

$$\phi'' + \frac{1}{2}Lef\phi' + LePe_\xi[f'\phi'' + f''\phi'] = 0 \tag{10}$$

The boundary conditions (5) transform into

$$\eta = 0: \ f = 0, \theta = 1, \phi = 1,$$

$$\eta \to \infty: \ f' = 1, \theta = 0, \phi = 0 \tag{11}$$

The important parameters involved in the present study are the radiation parameter $R = \frac{4\sigma}{3k_0 k}(T_w - T_\infty)^3$, temperature difference $C_T = \frac{T_\infty}{T_w - T_\infty}$, the local Peclet number $Pe_x = \frac{U_\infty x}{\alpha}$ the local Darcy-Rayleigh number $Ra_x = \frac{gK\beta_T\theta_w x}{\alpha\nu}$, which is defined with reference to the temperature difference alone, $Pe = \frac{U_\infty d}{\alpha}$ and $Ra = \frac{gK\beta_T\theta_w d}{\alpha\nu}$, are the pore diameter-dependent Peclet and

Rayleigh number, respectively. The inertial parameter is $F_0 Pe = \frac{c\sqrt{K}U_\infty}{\nu}$ (in the present study $F_0 Pe = 1.0$) the buoyancy ratio is $N = \frac{\beta_C \phi_w}{\beta_T \theta_w}$ and the diffusivity ratio is $Le = \alpha / D$. The Lewis number is nothing but the ratio of the Schmidt number ν / D and Prandtl number ν / α. The flow governing parameter is Ra / Pe and is independent of x. $Ra / Pe = 0$ represents the forced convection flow. The flow asymptotically reaches the free convection flow limit as this parameter tends to ∞. Pe_γ and Pe_ξ represent thermal and solutal dispersion parameters, respectively, and are defined here as $Pe_\gamma = \frac{\gamma U_\infty d}{\alpha}$ and $Pe_\xi = \frac{\xi U_\infty d}{\alpha}$. In the present investigation, we consider the thermal and solutal dispersion parameters Pe_γ and Pe_ξ with γ and ξ included in the parameters. In Eq. (8) the positive and negative signs represent aiding and opposing flows, respectively, $N > 0$ indicates the aiding buoyancy and $N < 0$ indicates the opposing buoyancy.

The heat and mass transfer coefficients, in terms of the Nusselt and Sherwood numbers in the presence of radiation and thermal and solutal dispersion diffusivities, can be written as

$$q_w = -k_c \frac{\partial T}{\partial y} - \frac{4\sigma}{3k_0} \frac{\partial T^4}{\partial y}\bigg|_{y=0},$$

q_w the effect heat transfer coefficient; $k_c = k + k_d$ where k_c effective thermal conductivity; k_d the dispersion thermal conductivity

$$j_w = -D_c \frac{\partial C}{\partial y}\bigg|_{y=0},$$

j_w the convective mass transfer coefficient; D_c mass diffusivity

$$\frac{Nu}{Pe_x^{1/2}} = \frac{q_w}{T_w - T_\infty}\frac{x}{k_e} = -[1 + Pe_\gamma f'(0) + \frac{4}{3}R(C_T + \theta(0))^3]\theta'(0) \quad (12)$$

$$\frac{Sh}{Pe_x^{1/2}} = \frac{j_w x}{D_c(C_w - C_\infty)} = -[1 + Pe_\xi f'(0)]\varphi'(0), \quad (13)$$

when $R = 0$, $Pe_\gamma = Pe_\xi = 0$, Eqs. (12)-(13) become $\frac{Nu}{Pe_x^{1/2}} = -\theta'(0)$ and $\frac{Sh}{Pe_x^{1/2}} = -\phi'(0)$. For $Pe_\gamma = Pe_\xi = 0$, $R \neq 0$ then

$$\frac{Nu}{Pe_x^{1/2}} = -[1 + \frac{4}{3}R(C_T + \theta(0))^3]\theta'(0)$$

3. Results and Discussion

The resulting ordinary differential Eqns. (8)-(10) are integrated by giving appropriate initial guess values for $f'(0)$, $\theta'(0)$ and $\phi'(0)$ to match the values with the corresponding boundary conditions at $f'(\infty)$, $\theta(\infty)$ and $\phi(\infty)$ respectively.

NAG software (D02HAFE routine) is used for integrating the corresponding first-order system of equations and shooting and matching the initial and boundary conditions. The step size $\Delta\eta = 0.05$ is used while obtaining the numerical solution with $\eta_{max} = 12$ and five –decimal accuracy as the criterion for convergence. Extensive calculations have been performed to obtain the flow, temperature and concentration fields for a wide range of parameter $0 \le Ra/Pe \le 100$, $0 \le R \le 1.0$, $F_0 Pe = 1.0$, $N = -0.5,\ 1.0,\ 0.1 \le Le \le 100,\ C_T = 0.01$, $0 \le Pe_\gamma \le 5,$ and $0 \le Pe_\xi \le 5.$ With $R = 0,$ $F_0 Pe = 0,$ (Darcian case), $Pe_\gamma = 0$ and $Pe_\xi = 0$ the present problem reduces to heat and mass transfer by Darcian mixed convection in porous media analyzed by Lia [4], and for $F_0 Pe = 1.0$ with variation of another parameter compared with Murthy (2000).

Aiding flow: when buoyancy is aiding the flow, for $N > 0$ (aiding buoyancy case) the tangential velocity evolves from nonzero wall velocity to uniform freestream velocity for all values of $N > 0$. The vertical component of velocity attains negative values near the wall and well inside the boundary layer.

The wall temperature gradient values for $F_0 Pe = 1.0$ for two values of $N = -0.5$ and $N = 1.0$ are presented in Tables (II-III). The value of $f'(0)$ is independent on R. From these tables, it is clear that $f'(0)$ depends on the buoyancy ratio N. The variation of the heat transfer coefficient with Ra/Pe for nonzero values of Pe_γ is studied for a wide range of values of $Le.$ The effect of thermal dispersion on the heat transfer is studied keeping $Pe_\xi = 0$. Consistent with the results presented in Lai and Kulacki (1991b), the value of $-\theta'(0)$ decreases as the thermal dispersion coefficient Pe_γ increases.

Table 1: Values for $f'(0)$ and $-\theta'(0)$ for varying Ra/Pe, Pe_γ with $Pe_\xi = 0$, $Le = 1$

		Murthy (2000)			Present work			
$\frac{Ra}{Pe}$	$f'(0)$	$Pe_\gamma = 0$	$Pe_\gamma = 1$	$Pe_\gamma = 5$	$f'(0)$	$Pe_\gamma = 0$	$Pe_\gamma = 1$	$Pe_\gamma = 5$
0.0	1.0	0.56421	0.39895	0.23044	1.0	0.56419	0.39894	0.23045
1.0	1.15834	0.59224	0.40279	0.23068	1.15831	0.59223	0.40277	0.23066
5.0	1.67946	0.67933	0.41884	0.23564	1.67944	0.67930	0.41881	0.23559
10	2.19261	0.75803	0.43484	0.24077	2.19258	0.75804	0.43481	0.24072
20	3.1000	0.87062	0.45627	0.24688	3.0	0.87055	0.45622	0.24678
50	4.72062	1.07684	0.48784	0.25447	4.72014	1.07681	0.48782	0.25442

Table 2: Variation of $-\theta'(0)$ for varying of R, Ra/Pe, Pe_γ and Le with $Pe_\xi = 0$, $N = -0.5$

			$Le = 1.0$			$Le = 10$		
R	$\frac{Ra}{Pe}$	$f'(0)$	$Pe_\gamma = 0.0$	$Pe_\gamma = 1.0$	$Pe_\gamma = 5.0$	$Pe_\gamma = 0.0$	$Pe_\gamma = 1.0$	$Pe_\gamma = 5.0$
	0.0	1.0	0.56419	0.39894	0.23045	0.56419	0.39894	0.23045
0.0	1.0	1.15831	0.59223	0.40277	0.23066	0.60540	0.41525	0.23699
	5.0	1.67944	0.67930	0.41881	0.23559	0.72436	0.43500	0.24041
	10	2.19258	0.75804	0.43483	0.24072	0.82473	0.45104	0.26959
	20	3.0	0.87055	0.45622	0.24678	0.96171	0.47823	0.30644
	50	4.72014	1.07681	0.48782	0.25442	1.20301	0.50729	0.32186
	0.0	1.0	0.37535	0.31573	0.21125	0.37535	0.31573	0.21125
	1.0	1.15831	0.39641	0.32513	0.21387	0.40513	0.33464	0.21952
	5.0	1.67944	0.46052	0.35362	0.22330	0.48921	0.38192	0.23688
	10	2.19258	0.51733	0.37732	0.23079	0.55896	0.41443	0.25596
	20	3.0	0.59736	0.40693	0.23907	0.65332	0.45012	0.27931
0.5	50	4.72014	0.74209	0.44934	0.24913	0.81843	0.48891	0.30564
	0.0	1.0	0.29251	0.26541	0.19552	0.29251	0.26541	0.19552
	1.0	1.15831	0.31030	0.27666	0.19979	0.31701	0.28432	0.20490
	5.0	1.67944	0.36366	0.30942	0.21250	0.38517	0.33254	0.22500
	10	2.19258	0.41031	0.33615	0.22283	0.43379	0.35999	0.24186
	20	3.0	0.47539	0.36943	0.23194	0.51853	0.40153	0.27311
1.0	50	4.72014	0.59211	0.41781	0.24411	0.65721	0.45391	0.29655

Also for large Pe_γ, in a very small region near the wall, temperature gradient is greatly increased and as a result heat transfer is greatly enhanced due to thermal dispersion. The value of $-\theta'(0)$ decreases as the radiation parameter R increases. The value $-\theta'(0)$ increases with increase Ra/Pe, and the value of Le enhances of $-\theta'(0)$ when $N = -0.5$, but, it reduce when $N = 1.0$.

The effect of radiation and solutal dispersion on the mass transfer coefficient has been analyzed keeping $Pe_\gamma = 0$. The values of $-\phi'(0)$ have been tabulated for $F_0 Pe = 1.0$, $N = -0.5$ and $N = 1.0$ in Tables (VI-V). Analogous to the pure thermal convection process, the value of $-\phi'(0)$ decreases with increasing values of Pe_ξ. But the increase value of radiation parameter R enhance $-\phi'(0)$ with fixed

Table 3: Variation of $-\theta'(0)$ for varying of R, Ra/Pe, Pe_γ and Le with $Pe_\xi = 0$, $N = 1.0$.

			$Le = 1.0$			$Le = 10$		
R	$\frac{Ra}{Pe}$	$f'(0)$	$Pe_\gamma = 0$	$Pe_\gamma = 1$	$Pe_\gamma = 5$	$Pe_\gamma = 0$	$Pe_\gamma = 1$	$Pe_\gamma = 5$
0.0	0.0	1.0	0.56419	0.39894	0.23045	0.56419	0.39894	0.23045
	1.0	1.56155	0.66027	0.38933	0.19845	0.63766	0.37046	0.18999
	5.0	3.00000	0.87055	0.37742	0.16944	0.80833	0.34066	0.15702
	10	4.21699	1.02028	0.37172	0.16080	0.86751	0.33579	0.14895
	20	6.00000	1.20974	0.36603	0.15505	0.99757	0.32437	0.14366
	50	9.61187	1.52680	0.35883	0.15054	1.11689	0.31386	0.13973
0.5	0.0	1.0	0.37535	0.31573	0.21125	0.37535	0.31573	0.21125
	1.0	1.56155	0.43978	0.32316	0.18713	0.42471	0.30825	0.17940
	5.0	3.00000	0.53500	0.33388	0.16419	0.53958	0.30297	0.15247
	10	4.21699	0.68033	0.33807	0.15724	0.64185	0.28443	0.15016
	20	6.00000	0.80676	0.34092	0.15264	0.78793	0.26977	0.14879
	50	9.61187	1.01826	0.34241	0.14909	0.99985	0.25318	0.14553
1.0	0.0	1.0	0.29251	0.26541	0.19552	0.29251	0.26541	0.19552
	1.0	1.56155	0.34276	0.27935	0.17729	0.33107	0.26706	0.17019
	5.0	3.00000	0.45234	0.30110	0.15934	0.42112	0.26706	0.14824
	10	4.21699	0.53026	0.31120	0.15388	0.40053	0.27455	0.13722
	20	6.00000	0.62880	0.31979	0.15033	0.38839	0.25311	0.13019
	50	9.61187	0.79365	0.32782	0.14768	0.36875	0.23379	0.12731

parameter R enhance $-\phi'(0)$ with fixed the other parameters. Interestingly, at large Pe_ξ, for large values of Ra/Pe, in a relatively large region (larger than that observed for thermal gradients) near the wall, the concentration gradient is greatly increased. But, against this expectation peculiar behavior in the mass transfer coefficient is observed (see Murthy (2000)). The imbalance between the Lewis number and buoyancy parameter influence more against the enhancement of the mass transfer results.

For $Pe_\xi = 0$, the value of $-\phi'(0)$ increases with increasing values of Ra/Pe for all values of Le and N. For large Pe_ξ, the value of $-\phi'(0)$ decreases rapidly to near zero values with increasing Ra/Pe.

The variation of $-\dfrac{Nu}{Pe_x^{1/2}}$ with R and Ra/Pe in the opposing flow is presented in Table (VI) with $F_0 Pe = 1.0$ for different value of ($Pe_\gamma = 0$, 1, 5) and ($N = -0.5$, 1.0). Thermal dispersion and radiation

Table 4: **Variation of $-\phi'(0)$ for varying of R, Ra/Pe, Pe_ξ and Le with $Pe_\gamma = 0$, $N = -0.5$**

			$Le = 1.0$			$Le = 10$		
R	$\frac{Ra}{Pe}$	$f'(0)$	$Pe_\xi = 0$	$Pe_\xi = 1$	$Pe_\xi = 5$	$Pe_\xi = 0$	$Pe_\xi = 1$	$Pe_\xi = 5$
0.0	0.0	1.0	0.56419	0.39894	0.23045	1.78412	0.53793	0.24987
	1.0	1.15831	0.59223	0.38837	0.20630	1.93287	0.51217	0.22082
	5.0	1.67944	0.67930	0.35547	0.14588	2.35336	0.44638	0.15966
	10	2.19258	0.75804	0.32543	0.10350	3.21597	0.40371	0.15280
	20	3.0	0.87055	0.28223	0.06659	3.97841	0.38673	0.14321
	50	4.72014	1.07681	0.21355	0.04841	5.35379	0.31888	0.13857
0.5	0.0	1.0	0.56419	0.39894	0.23045	1.78412	0.53793	0.24987
	1.0	1.15831	0.59663	0.39267	0.20859	1.94121	0.51941	0.22355
	5.0	1.67944	0.69502	0.36934	0.15210	2.37802	0.46650	0.15978
	10	2.19258	0.78190	0.34494	0.11098	3.86879	0.41784	0.14591
	20	3.0	0.90393	0.30698	0.07359	4.68315	0.35397	0.13997
	50	4.72014	1.12404	0.24099	0.05219	6.11943	0.31756	0.13011
1.0	0.0	1.0	0.56419	0.39894	0.23045	1.78412	0.53793	0.24987
	1.0	1.15831	0.59986	0.39605	0.21049	1.94586	0.52485	0.22580
	5.0	1.67944	0.70629	0.38034	0.15742	2.39143	0.48196	0.16572
	10	2.19258	0.79877	0.36061	0.11756	4.33829	0.43527	0.15175
	20	3.0	0.92723	0.32724	0.07983	5.21537	0.40074	0.14462
	50	4.72014	1.19315	0.26425	0.05579	6.97311	0.34769	0.13989

enhances the heat transfer rate in both $N = -0.5$, 1.0 for all values of $Le > 0$. Interestingly, for fixed Le, and nonzero Pe_γ, there exists one critical value of Ra/Pe before which the $-\frac{Nu}{Pe_x^{1/2}}$ for $N = 1.0$ is more than that for $N = -0.5$ and after which its reverse is seen. The $-\frac{Sh}{Pe_x^{1/2}}$ is presented against Ra/Pe for $F_0 Pe = 1.0$ and for six combinations of Pe_ξ and N in Table (VII).

Figure 1 illustrate velocity profiles as a function of the similarity variable η for case aiding buoyancy. Fig. 1 shows the velocity distribution for varying values of radiation parameter R for non-Darcy case ($F_0 Pe = 1.0$), $Pe_\gamma = Pe_\xi = 0$ (aiding flow) with $Le = 1.0$, $N = -0.5$. From this figure we, observe that the velocity profiles increases with increase of parameter radiation. Also, we observe that the increases of Ra/Pe enhances the velocity at fixed the other parameters.

Table 5: Variation of $-\phi'(0)$ for varying of R, Ra/Pe, Pe_ξ and Le with $Pe_\gamma = 0$, $N = 1.0$

			$Le = 1.0$			$Le = 10$		
R	$\frac{Ra}{Pe}$	$f'(0)$	$Pe_\xi = 0$	$Pe_\xi = 1$	$Pe_\xi = 5$	$Pe_\xi = 0$	$Pe_\xi = 1$	$Pe_\xi = 5$
0.0	0.0	1.0	0.56419	0.39894	0.23045	1.78412	0.53793	0.24987
	1.0	1.56155	0.66027	0.38933	0.19845	2.13811	0.47766	0.20788
	5.0	3.00000	0.87055	0.37742	0.16944	2.88656	0.42210	0.17279
	10	4.21699	1.02028	0.37172	0.16080	3.40615	0.40571	0.16533
	20	6.00000	1.20974	0.36603	0.15505	4.05482	0.38722	0.15669
	50	9.61187	1.52680	0.35883	0.15054	5.13491	0.36101	0.14991
0.5	0.0	1.0	0.56519	0.39894	0.23045	1.78412	0.53793	0.24987
	1.0	1.56155	0.66373	0.39235	0.19982	2.14484	0.48244	0.20947
	5.0	3.00000	0.87932	0.38304	0.17134	2.90218	0.42976	0.17485
	10	4.21699	1.03186	0.37778	0.16261	3.46593	0.41079	0.16797
	20	6.00000	1.22435	0.37206	0.15668	4.11205	0.39998	0.15825
	50	9.61187	1.54583	0.36436	0.15192	5.13585	0.36979	0.15011
1.0	0.0	1.0	0.56419	0.39894	0.23045	1.78412	0.53793	0.24987
	1.0	1.56155	0.66632	0.39477	0.20098	2.14861	0.48615	0.21080
	5.0	3.00000	0.88599	0.38772	0.17297	2.91083	0.43604	0.17662
	10	4.21699	1.04074	0.38289	0.16417	3.49215	0.41537	0.16996
	20	6.00000	1.23558	0.37720	0.15809	4.17499	0.40192	0.16007
	50	9.61187	1.56049	0.36909	0.15310	5.24193	0.38129	0.15215

Table 6: Variation of $-\frac{Nu}{Pe_x^{1/2}}$ for varying of R, N, Le, Ra/Pe, Pe_γ with $Pe_\xi = 0$, $F_0 Pe = 1$

			$Le = 1.0$			$Le = 10.0$		
N	R	$\frac{Ra}{Pe}$	$Pe_\gamma = 0$	$Pe_\gamma = 1$	$Pe_\gamma = 5$	$Pe_\gamma = 0$	$Pe_\gamma = 1$	$Pe_\gamma = 5$
-0.5	0.0	0.1	0.56118	0.79052	1.36380	0.55964	0.78747	1.35872
		1.0	0.53189	0.72213	1.19033	0.51409	0.68810	1.13100
-0.5	0.5	0.1	0.62932	0.84034	1.39331	0.62758	0.83724	1.38830
		1.0	0.59167	0.76552	1.21560	0.57084	0.73006	1.15643
-0.5	1.0	0.1	0.68976	0.88688	1.42212	0.68784	0.88372	1.41709
		1.0	0.64454	0.80596	1.24027	0.62109	0.76939	1.18136
1.0	0.0	0.1	0.55187	0.77391	1.33878	0.55500	0.78007	1.34914
		1.0	0.37342	0.47189	0.76294	0.42625	0.55561	0.90153
1.0	0.5	0.1	0.61920	0.82401	1.36885	0.62278	0.83030	1.37913
		1.0	0.41504	0.51168	0.80281	0.47679	0.60257	0.95278
1.0	1.0	0.1	0.67901	0.87074	1.39816	0.68295	0.87712	1.40829
		1.0	0.44783	0.53173	.82759	0.52334	0.64483	0.99189

Table 7: Variation of $-\frac{Sh}{Pe_x^{1/2}}$ for varying of R, N, Le, Ra/Pe, Pe_ξ with $Pe_\gamma = 0$, $F_0 Pe = 1$

			$Le = 1.0$			$Le = 10.0$		
N	R	$\frac{Ra}{Pe}$	$Pe_\xi = 0.0$	$Pe_\xi = 1.0$	$Pe_\xi = 5.0$	$Pe_\xi = 0.0$	$Pe_\xi = 1.0$	$Pe_\xi = 5.0$
-0.5	0.0	0.1	0.56118	0.79346	1.37995	1.76759	1.07270	1.49863
		1.0	0.53189	0.74944	1.34570	1.60035	1.04181	1.48834
-0.5	0.5	0.1	0.56067	0.79244	1.37824	1.76654	1.07085	1.49650
		1.0	0.52621	0.73830	1.32616	1.58674	1.01985	1.46344
-0.5	1.0	0.1	0.56030	0.79165	1.37682	1.76594	1.06948	1.49479
		1.0	0.52193	0.72963	1.31021	1.57878	1.00364	1.44328
1.0	0.0	0.1	0.55187	0.77391	1.33878	1.73797	1.06233	1.46203
		1.0	0.37342	0.47189	0.76294	1.04066	2.53051	4.92592
1.0	0.5	0.1	0.55135	0.77287	1.33697	1.73687	1.06041	1.45983
		1.0	0.36167	0.45430	0.73287	1.00991	2.42579	3.54993
1.0	1.0	0.1	0.55096	0.77206	1.33550	1.73626	1.05898	1.45802
		1.0	0.35323	0.44155	0.71066	0.99160	2.35268	3.48426

The temperature profile for the case aiding buoyancy is presented in Fig. 2. It is evident from this figure the radiation parameter R enhances the temperature profiles. It can be seen that as the buoyancy parameter N increases, the temperature profiles decreases. Also, this figure clearly indicates the favorable influence of the thermal dispersion on the temperature profiles. The temperature profiles θ as a function of η increases with increase of thermal dispersion Pe_γ for $N = -0.5$, $N = 1.0$.

The effect of radiation parameter R, solutal dispersion Pe_ξ and buoyancy parameter N on concentration profiles is plotted in Fig. 3. From this figure, we observe the concentration profiles for the case aiding buoyancy increases with increase the solutal dispersion Pe_ξ, also, it increase with radiation parameter increase. It is noteworthy, from Fig. 3, that as the buoyancy parameter increases the concentration profiles decreases.

The heat transfer coefficient as a function of Lewis number Le for the without dispersion case $Pe_\gamma = Pe_\xi = 0$ is plotted in Fig. 4. From this figure it can be seen that an increase in the value of the mixed convection and radiation parameter R increases the heat transfer rates. The heat transfer coefficient is observed to increase with the radiation parameter and diffusivity ratio in the opposing buoyancy case, whereas it decreases in the aiding buoyancy case. For fixed values of other parameters the magnitude of $\frac{Nu}{Pe_x^{1/2}}$ for $N = 1.0$ is higher than $N = -0.5$ for all values of Le considered in the study. This clearly indicates that the buoyancy ratio has significant effect on the heat transfer coefficient than the diffusivity ratio.

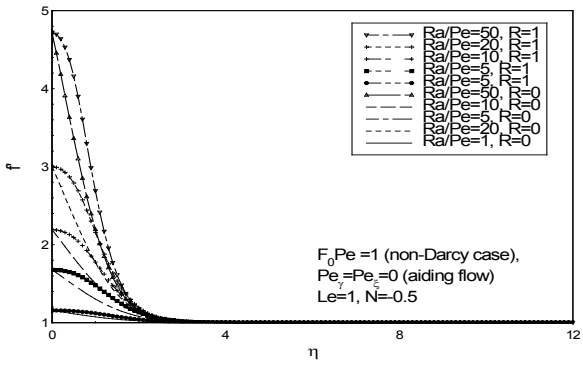

Fig.1 Non dimensional velocity profiles for varying of Ra/Pe, Le, N and R with C_T=0

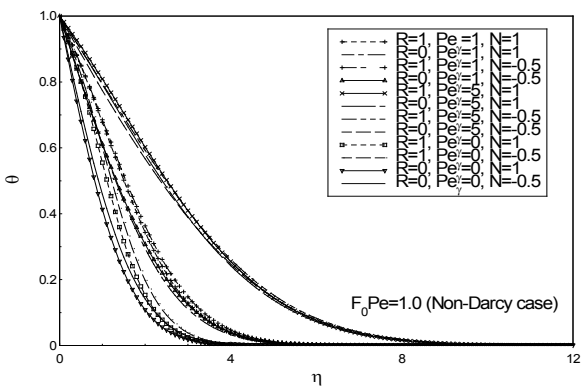

Fig.2: Variation of temperature profiles for varying N, R, and Pe_γ with Ra/Pe=1, Le=1, Pe_ξ=0

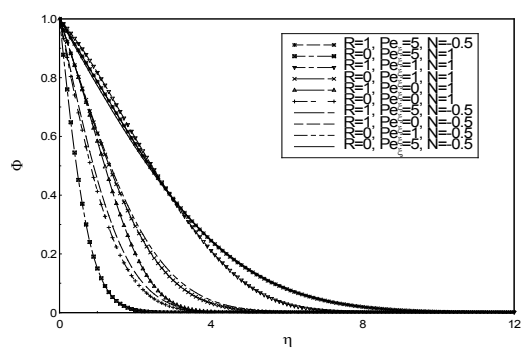

Fig. 3: Variation of concentration profiles for varying R, Pe_ξ, N with Ra/Pe=1, Pe_γ=0, Le=1, CT=0.01

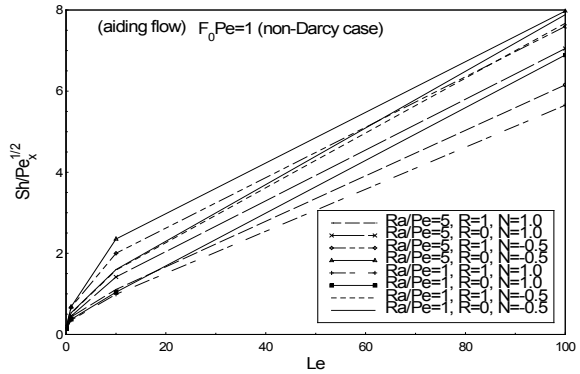

Fig.4: Heat transfer coefficient as a function of (Lewis number FPe=1, Pe_γ= Pe_ξ=0 (aiding flow

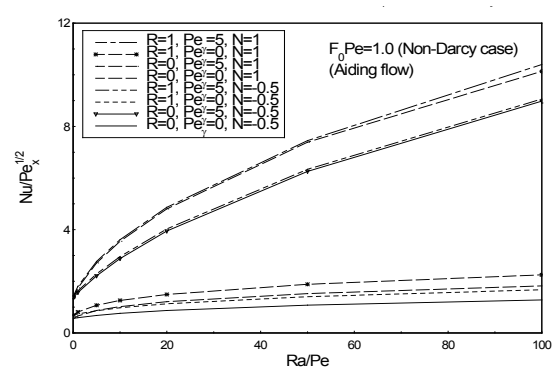

Fig.5: Mass transfer coefficient for varying Ra/Pe, R and N with Pe_γ= Pe_ξ=0, C_T=0.01

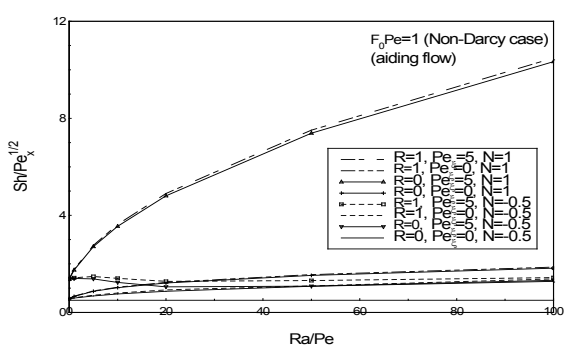

Fig.6: Variation of heat transfer coefficient for .varying R, Pe_γ, N withLe=1, Pe_ξ=0 and C_T=0.01

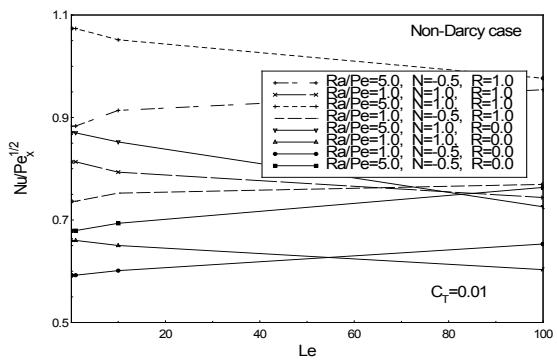

Fig.7: Variation of mass transfer coefficient for .varying R, Pe_γ=0, N withLe=1, Pe_ξ=0 and C_T=0.01

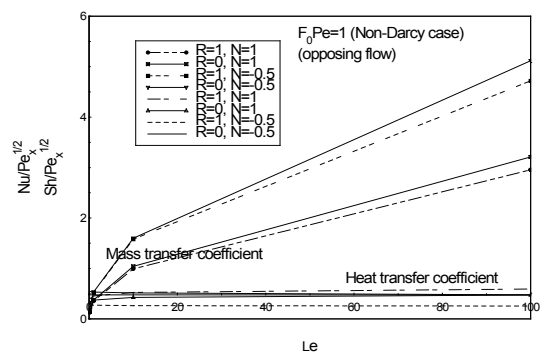

Fig.8: Variation of heat transfer coefficient for varying R, Pe_γ, N withLe=1, Pe_ξ=0 and C_T=0.01.

Fig. 5 clearly indicate the favorable effect of the Lewis number on the mass transfer coefficient in both opposing and aiding buoyancies, but the effect of radiation parameter reduced the mass transfer coefficient. Uniform trend in the Sherwood number results is observed with increase in the buoyancy ratio N from –0.5 to 1.0.

The variation of the heat transfer coefficient with Ra/Pe for nonzero values of Pe_γ is studied for a wide range of values of Le and plotted in Fig. 6. For $Le = 1.0$ this figure clearly indicate the favorable influence of thermal dispersion and radiation on the heat transfer results. The value of $-\frac{Nu}{Pe_x^{1/2}}$ increases with increasing Ra/Pe. Aiding buoyancy and radiation parameter R favors the heat transfer, whereas this favorable action is aided by $Le = 1.0$ when $N = -0.5$, and is suppressed by the $Le = 1.0$ when $N = 1.0$. These results are in agreement with the results reported by Murthy (2000) and Lai (1991).

The complex interaction between R, N, Pe_ξ and Ra/Pe show complex behavior for $-\frac{Sh}{Pe_x^{1/2}}$ curve. The result presented in Fig. 7 with $Le = 1.0$, $F_0 Pe = 1.0$ and $Pe_\gamma = 0$. In the case of aiding buoyancy, when $Le = 1.0$, the mass transfer coefficient increases with Ra/Pe and, the dispersion mechanism augments the mass transfer, when $N = -0.5$, $-\frac{Sh}{Pe_x^{1/2}}$ increases with R and Ra/Pe for $Pe_\xi = 0$. When $Pe_\xi = 5$, it increases with Ra/Pe upto the value 5 and the decreases thereafter. Its value becomes less than the corresponding value for $Pe_\xi = 1.0$ from $Ra/Pe = 20$ on wards: it may be inferred that the strength of the solutal dispersion becomes insignificant at higher values of Ra/Pe in the case of opposing buoyancy.

Opposing flow. The flow field becomes more complex when the freestream flow is opposing the buoyancy. Like in the aiding flow case, the wall velocity depends only the inertial, radiation parameters and buoyancy ratio. Flow separation is the most common

ratio. Flow separation is the most common feature observed in the opposing flows. The flow separation point also depends on the buoyancy ratio. In the Forchheimer flow ($F_0 Pe = 1$) the occurrence of the flow separation is delayed the separation points are observed to occur at $Ra/Pe = 0.1$, 1 for $N = -0.5$, 1.0 and $R = 0$, 0.5, 1.0. The presence of the radiation, thermal and solutal dispersion diffusivity will not alter the point of flow separation in non-Darcy flow. The heat and mass transfer coefficients in opposing flow are presented in Fig. 8. As expected the heat transfer decreases with Le for opposing buoyancy, where as it increases with Le for aiding buoyancy. It is just a reverse mechanism to the aiding flow case and is clearly seen also, in Fig. 8. The $-\frac{Sh}{Pe_x^{1/2}}$ values for the opposing buoyancy are at higher level than those for aiding buoyancy. It is evident from the Fig. 8 that the mass transfer coefficient increases with Le also, the $-\frac{Sh}{Pe_x^{1/2}}$ values in opposing buoyancy are higher level than those in aiding buoyancy. The radiation parameter enhance the heat transfer coefficient and reduce the mass transfer coefficient. Aiding buoyancy is hindrance to the freestream flow in the opposing flow case, so a reduction in the transport quantities is observed.

Concluding Remarks

Similarity solution for hydrodynamic dispersion-radiation in mixed convection heat and mass transfer near vertical surface embedded in a porous medium has been presented. The heat and mass transfer in the boundary layer region has been analyzed for aiding and opposing buoyancies in both the aiding and opposing flows. The structure of the flow, temperature and concentration fields in the non-Darcy porous media are governed by complex interactions among the diffusion rate Le and buoyancy ratio N in addition to the flow driving parameter Ra/Pe. For small values of Le in the opposing buoyancy, flow reversal near the wall is observed. The heat transfer coefficient always increases with Ra/Pe. Thermal dispersion-radiation favors the heat transfer. As Le increases the effect of solutal dispersion on the non-dimensional mass transfer coefficient becomes less predictable in both aiding and opposing buoyancies. In the opposing flow case, the flow separation point is observed to depend on the inertial parameter and buoyancy ratio. A reduction in the heat and mass transfer coefficients is seen with increasing values of Ra/Pe. The Lewis number has complex impact on the heat and mass transfer mechanism.

Nomenclature

c inertial coefficient

C concentration

C_T temperature ratio

d particle diameter

D mass diffusivity

D_C effective mass diffusivity

f dimensionless stream function

$F_0 Pe$ parameter representing non-Darcian effects

g acceleration due to gravity

k thermal conductivity

K permeability coefficient of the porous medium

Le Lewis number

N buoyancy ratio

$\frac{Nu}{Pe_x^{1/2}}$ non-dimensional heat transfer coefficient

Pe_x local Peclet number

Pe_γ parameter representing thermal dispersion effects

Pe_ξ parameter representing solutal dispersion effects

q^r radiative flux

R radiation parameter

Ra_x modified Rayleigh number

$\frac{Sh}{Pe_x^{1/2}}$ non-dimensional mass transfer coefficient

T temperature

u, v velocity components in x and directions

x, y axial and normal coordinates

α thermal diffusivity

α_{ff} effective of thermal diffusivity

β_T coefficient of thermal expansion

β_C coefficient of solutal expansion

η dimensionless distance

θ non-dimensional temperature

ν kinematic viscosity

ϕ non-dimensional concentration

γ coefficient of dispersion thern diffusivity

ξ coefficient of dispersion solu diffusivity

ψ stream function

Acknowledgements

We are thankful to the deanship of scientific research and department of Mathematics, College of Science, Al-Zulfi, Majmaah University, Kingdom of Saudi Arabia for providing all facilities in the completion of this work.

References

[1] Bejan, A. and Khair, K. R.,(1985). Heat and mass transfer by natural convection in a porous medium. Int. J. Heat Mass Transfer 28, pp. 909-918.

[2] Murthy, P. V. S. N. and Singh, P.(1999). Heat and mass transfer by natural convection in a non-Darcy porous medium. Acta Mech. 136, pp. 135-142.

[3] Merkin, J. H., (1980). Mixed convection boundary layer flow on a surface in a saturated porous medium. J. Engng. Math. 14, pp. 301-313.

[4] Lai, F. C.,(1991). Coupled heat and mass transfer by mixed convection from a vertical plate in a saturated porous medium. Int. Commun. Heat Mass Tranfer, 18, pp. 93-106.

[5] Lai, F. C. and Kulacki, F. A.,(1991b). Non-Darcy mixed convection along a vertical wall in saturated porous medium. ASME J. Heat Transfer, 113, pp. 252-255.

[6] Amiri, A. and Vafai, K.,(1994). Analysis of dispersion effects and non-theormal equilibrium, non-Darcian variable porosity incomressible flow through porous media." Int. J. Heat Mass Transfer, 37, pp. 936-954.

[7] Murthy, P.V.S.N. and Singh, P.,(1997). Thermal dispersion effects on non-Darcy natural convection over horizontal plate surface mass flux. Arch. Appl. Meck. 67, pp. 487-495.

[8] Karimi-Fard, M., Charrier-Mojtabi, M. C. and Vafai, K.,(1997). Non-Darcian effects on double-diffusive convection within a porous medium. Numer. Heat

Transfer, Part A, 31, pp. 837-852.

[9] Dagan, G.,(1972). Some aspects of heat and mass transport in porous media. Development in soil science:Fundamental of transport phennomena in porous media. Int. Association for Hydraulic Research, Elsevier, London, pp. 55-63.

[10] Telles, R. S. and Trevisan, O. V.,(1993) Dispersion in heat and mass transfer natural convection along vertical boundaries in porous media. Int. J. Heat Mass Transfer, 36, pp. 1357.

[11] Murthy, P.V. S. N. and Singh, P.,(1997). Thermal dispersion effects on non-Darcy natural convection with lateral mass flux. Heat Mass Transfer, 33, pp. 1-5.

[12] Murthy, P. V. S. N., (2000). Effect of double dispersion on mixed convection heat and mass transfer in non-Darcy porous medium." ASME J. vol. 122, pp. 476-484.

[13] Mansour, M. A. and El-Amin, M. F. (1999). Thermal dispersion effects on non-Darcy axisymmetric free convection in a saturated porous medium with lateral mass transfer . Applied Mechanics and Engineering, vol. 4, No. 4, pp. 727-737.

[14] El-Amin, M. F., (2004). Double dispersion effects on natural convection heat and mass transfer in non-Darcy porous medium. Applied Mathematics and Computation, 156, pp. 1-17 .

[15] Hossain., M.A. and Takhar, H. S., (1996). Radiation effect on mixed convection along a vertical plate with uniform surface temperature. Heat Mass Transfer, 31, pp. 243-248.

[16] Raptis, A., (1998). Radiation and free convection flow through a porous medium."Int. Commun. Heat Mass Transfer 25; 289-295.

[17] Mohammdien, A.A. and El-Amin, M. F., (2000). Thermal dispersion-radiation effects on non-Darcy natural convection in a fluid saturated porous medium.Transport in Porous Media, 40, 2, pp. 153.

[18] El-Hakiem, M. A. and El-Amin, M. F.,(2001) "Thermal radiation effect on non-Darcy natural convection with lateral mass transfer."Heat and Mass Transfer, 37, pp. 161-165.

[19] El-Hakiem, M. A.,(2009). "Radiative effects on non-Darcy natural convection from a heated vertical plate in saturated porous media with mass transfer for non-Newtonian fluid" J. Porous Media, vol. 12, no. 1, pp. 89-99.

[20] Chamkh, A. J., El—Kabeir, S. M. M. and Rashad, A. M.,(2011). "Heat and mass tramsfer by non-Darcy free convection from a vertical cylinder embedded in porous media with a temperature dependent viscosity." INT. J. NUMER METHOD & FLF, vol. 21, no. 7, pp. 847-863.

[21] Vanishree, R. K.,(2010)."Effect of rotation on thermal convection in an anisotropic porousmedium with temperature dependent viscosity." Trans Porous Media, vol. 81, no. 1, pp.73-87

[22] El-Hakiem, M. A., Rashad, A. M. and Abdou, M. M. M., (2011)."Natural convection boundary layer of non-Newtonian fluid about a permeable vertical Cone embedded in porous medium saturated with a nanofluid." Computer & Mathematics with applications, vol. 62, issue 8, pp. 3140-3151.

[23] Chamkha, A.J., et.al.,(2013)."Coupled heat and mass transfer by MHD free convection flow along a vertical plate with streamwise temperature and species concentration variations", Heat Transfer Asian Reaserch Journal, 42(2), pp. 100-110.

[24] Nield, D.A., Bejan, A.,(2013). Convection in Porous Media, fourth edition, Springer, New York.

[25] Kairi, R.R.,et.al.,(2010). Effect of double dispersion on mixed convection heat and mass transfer in a non-Newtonian fluid-saturated non-Darcy porous medium, J. Porous Media 13 749-757.

Experimental Study of the Influence of Process Conditions on Tubular Reactor Performance

M.K. Al Mesfer
Chemical Engg. Deptt., College of Engineering, King Khalid University, P.O.Box 394 Abha 61411 KSA.
almesfer@kku.edu.sa

M. Danish*
Chemical Engg. Deptt., College of Engineering, King Khalid University, P.O.Box 394 Abha 61411 KSA.
mdansh@kku.edu.sa

Abstract
This work presents an experimental study of the saponification reaction of ethyl acetate by sodium hydroxide in a tubular reactor at 1 atmosphere (atm) of pressure. The objective of this study is to analyze the effect of operating conditions on the rate constant and conversion in order to explore the tubular reactor performance. The temperature, reactant flow rate, and residence time are the parameters considered for analyzing the reactor performance. The steady-state conversion is achieved after a period of 30 minutes. Conversion decreases with the increased reactant flow rate, owing to the resulting decrease in residence time. The rate constant first decreases and then increases with feed flow rate. The rate constant and conversion increase with increased temperature within the studied temperature range. The residence time declines with increased reactants flow rates leading to decreased NaOH conversion. The obtained NaOH conversion values at different temperatures have been compared with literature data. The outcomes of this study may be useful in maximizing the conversion of ethyl acetate saponification reaction for industrial scale synthesis .of sodium acetate and ethanol synthesis in a tubular reactor

Keywords: Saponification; Plug flow reactor (PFR); Conductivity; Conversion; Hydrolysis.

1. Introduction

Several types of reactors are used in chemical or petrochemical industries. Plug flow reactors (PFRs), also known as continuous tubular reactors, play a key role in chemical industries. Tubular reactors are often used when continuous operation is required but back-mixing of products and reactants is not desired. The use of plug flow reactors becomes especially important when continuous large-scale production is needed. PFRs are associated with high volumetric unit conversion because the occurrence of side reactions is minimal. In plug flow reactors, reactants are fed from one end of reactor and flows continuously through the length of reactor as a series of plugs and the products are discharged from the other end of reactor.

Advantages of PFRs include high volumetric unit conversion and the capability of running for longer periods without any maintenance or less maintenance. For the same conversion and reaction conditions, PFR volume is usually lower than CSTR volume for isothermal reactions greater than zero order (Fogler, 2006). For the industrial

application, PFRs can be assembled as a single long tube or in the form of a coil. PFRs are extensively used in the industry for gaseous/liquid phase systems. PFRs are commonly used for gasoline production, oil cracking, oxidation of sulphur dioxide to sulphur trioxide, synthesis of ammonia and polymer manufacturing along with other applications.

According to Bursali et al., 2006, the hydrolysis of a fat or oil in alkaline condition produces soap and the reaction that occurs in alkaline conditions is known as saponification. Hydrolysis of an ester to produce an alcohol and the salt of a carboxylic acid, under basic conditions, is called saponification and it is normally referred as the reaction of antacid in the presence of fat/oil to produce soap. Saponification is the hydrolysis of ethyl acetate by sodium hydroxide to produce sodium acetate and ethanol. A lot of studies are available in the literature on the process improvement of this saponification reaction.

The effect of operating conditions on CSTR performance for ethyl acetate saponification has been investigated experimentally by Danish et al., 2015. The parameters selected for analysis were temperature, feed flow rate, residence time, reactor volume and stirrer rate. It was found that conversion decreases with increased flow rate due to decrease of residence time and agitation rate has a positive effect on the conversion and rate constant. It was also concluded that specific rate constant and conversion increases with increased temperature within the studied range.

The hydrolysis of ethyl acetate is one of the most important reactions, and it is characterized as second-order reaction in the literature (e.g. Kapoor, 2004). Various measurement techniques (Daniels et al., 1941; Schneider et al., 2005) have been used by several investigators at different temperatures to study saponification reaction. The techniques depend on the conductometric measurements to evaluate the composition at any time was reported by Walker, 1906 and this measurement approach circumvents regular removal of product samples for analysis.

Tsujikawa et al. 1966 estimated the rate constant and activated energy at an initial temperature of 25 ^{o}C as 0.112×10^{-3} m^3/mol. sec and 8.37 KJ/mol respectively for alkaline hydrolysis of ethyl acetate in a polyethylene batch reactor. It was also observed that the reaction rate reaction rate of ethyl acetate saponification is not expressed adequately by a second-order rate equation as given in literature (e.g Kapoor, 2004).

Other investigators focused their attention on online data recording, using a conductivity measurement technique to make the procedure much simpler. Researchers have conducted several studies on saponification reaction; the data exhibit wide scatter for the saponification of ethyl acetate with sodium hydroxide. Kuheli et al. 2011 conducted studies on the saponification of ethyl acetate by utilizing innovative conductivity-monitoring instruments. Rate constants of the saponification reaction at various

temperatures (range, 35˚C to 55˚C) were evaluated, and observed that outcomes were in agreement with some of the data reported in literature.

Ahmad et al. 2013 carried out a comparative study of ethyl acetate hydrolysis using full two level factorial design in batch (volume: $1x10^{-3}$ m^3 and plug flow reactors (volume: 0.4 $x10^{-3}$ m^3). The maximum fractional conversion of 0.97 was obtained at a residence time of 300 seconds in both type of reactors under optimum concentrations of NaOH (0.01 mol/L) and CH_3COONa (0.07 mol/L). It was also concluded that reaction conversion increases positively with increased absolute initial concentration of $CH_3COOC_2H_5$.

Saponification of ethyl acetate by sodium hydroxide to optimize the conversion in a continuous stirred tank reactor (CSTR) has been studied using two level factorial design and response surface methodology by Ullah et al., 2015. The maximum conversion of 96.71 % was obtained corresponding to sodium hydroxide and ethyl acetate concentration of 0.01 mol/L and 0.1 mol/L while it was suggested that the influence of feed ratio, agitation rate and temperature was insignificant which contradicts the findings (effect of reaction temperature on conversion) of other researchers (Wijayarathne et al., 2014; Danish et al., 2015). On other hand, the reactants concentration to maximize the conversion of sodium hydroxide reported by Ahmed et al. 2013 was different from the concentrations calculated by Ullah et al. 2015.

A comparative study of ethyl acetate saponification and an-oxidation-reduction reaction has been conducted in a batch and semibatch reactor by Grau et al., 2002. It was concluded that it is practicable to operate the reactor in both modes of operation to study the saponification reaction.

Hydrolysis of ethyl acetate by sodium hydroxide in a tubular reactor using Aspen Plus has been investigated by Wijayarathne and Wasalathilake, 2014. The simulated results were verified by the experimental data and it proves that predicted results were in agreement satisfactorily with experimental results. The model developed can be used as a reference to comprehend reaction kinetics of plug flow reactor. The objective of the current study is to investigate the influence of operating conditions on tubular reactor performance using hydrolysis of ethyl acetate by sodium hydroxide. The temperature, reactant flow rates and residence time are the parameters considered for analyzing the influence on steady-state conversion of NaOH and rate constant. The obtained result of sodium hydroxide conversion as a function of temperature of reaction mixture has been compared with literature data (Wijayarathne et al. 2014) in order to validate the outcome of current study.

2. Materials and methods

2.1 Chemicals

Analytical-grade reagents (AR) were used to carry out the research work. Ethyl acetate of purity 99.5% and sodium hydroxide of

concentration 98.0%-100% were utilized to conduct the experiments. The distilled water generated using distilled water unit (Type 2008,GFL) was used to prepare the solutions of sodium hydroxide NaOH (~0.1 M) and ethyl acetate $CH_3COOC_2H_5$ (~0.1 M).

2.2 Experimental Setup

The tubular reactor (reactor coil: length—20.9 m; internal diameter—$5.0x10^{-3}$ m; total volume of reactor V—$0.41x10^{-3}$ m^3) obtained from Armfield (U.K.) has been used for the experiments for the investigation as shown in Fig.1 and designed properly to facilitate the detailed study.

The tubular reactor in which the chemical reaction takes place made up of a pliable coil. The volume of the reactor in the form of coil is $0.41x10^{-3}$ m^3. The conductivity and temperature sensors are inserted into the gland for online data acquisition. In order to conduct an experiment at a fixed temperature, the reactor coil is immersed in water, which is maintained at a fixed temperature by temperature controller. Water enters the reactor through non-return valve and this valve prevents water draining back from reactor when pump is under switch off position.

The reactants i.e. NaOH and $CH_3COOC_2H_5$ enter the reactor coil from one end and leave the reactor vessel through the other end of the coil. The conductivity probe housing allows the conductivity probe to be fixed in the stream of products mixture coming out from the reactor coil. The progress of the hydrolysis reaction is recorded by conductivity probe as the conductivity of solution varies with conversion. The conductance of the reaction mixture varies with conversion. Priming vessel attached with reactor service unit is used to fill the reactor coil and returned back into the hot water circulator system. The reactants flow rates from the storage vessel

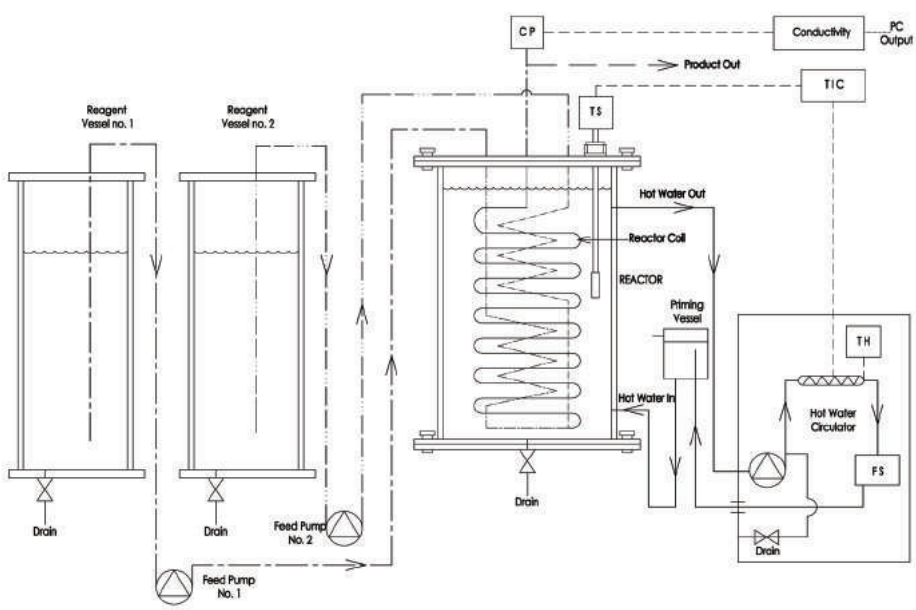

Fig. 1: Setup diagram of tubular reactor (adopted from Armfield, U.K.)

are controlled by using two peristaltic pumps; these pumps are calibrated so that any desired reactants flow rate can be adjusted.

2.3 Experimental Procedure

Solutions of sodium hydroxide and ethyl acetate were prepared to perform the experiments under different process conditions. Two peristaltic pumps were used to pump the reactant from feed tanks and enter the reactor vessel. The reactants pass through pre-heating coils submerged in the water; here, the reactants are individually brought up to the desired reaction temperature. The reactants are mixed together at the inlet of reactor coil and reaction proceeds as reaction mixture pass through the reactor coil.

After acquiring the required process conditions in the reactor, actual-time conductivity was recorded by the probe and displayed on control panel. The degree of conversion and hence, rate constant are tabulated by utilizing the conductivity data. One of the products of saponification reaction i.e. the sodium acetate ascribes for the conductivity after infinite time.

3. Results and Discussion

3.1 Steady-State Condition

Feed flow rates of 13.33×10^{-7} m^3/sec sodium hydroxide and 13.33×10^{-7} m^3/sec ethyl acetate were fixed using peristaltic pumps. Solutions of 0.1M NaOH and 0.1M $CH_3COOC_2H_5$ were used for conducting the experiments; and the saponification reaction were performed at a fixed temperature of 30°C. Conductance of reaction mixture was recorded

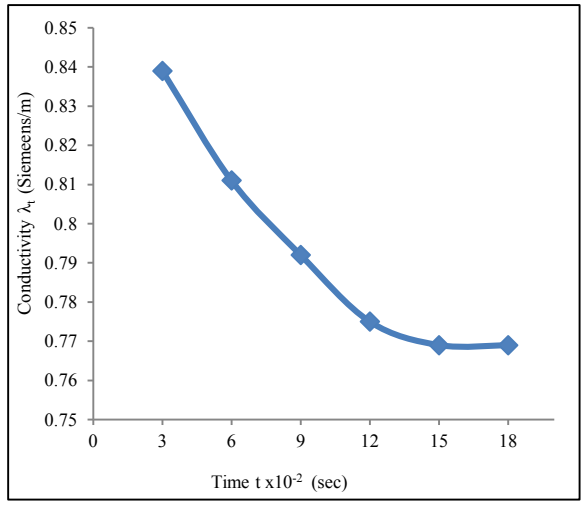

Fig.2: Conductivity versus time curve for $CH_3COOC_2H_5$ hydrolysis by NaOH

at 5-minute intervals until steady-state condition was reached. The steady-state condition was reached after 30 minutes as shown in Fig.2.

Sodium hydroxide and sodium acetate contributed conductance to the reaction mixture and on the other hand, ethyl acetate and ethyl alcohol do not. The sodium hydroxide solution conductivity at a given concentration and temperature is not equal to that of CH_3COON_A solution at the same concentration and reaction conversion.

The rate constant and reaction conversion were calculated at steady-state conditions. Reaction mixture conductivity decreases with time as the reaction proceeds, and it attains a steady-state value of conductivity after approximately 30 minutes. This occurs because as the reaction proceeds, the concentration of NaOH decreases, resulting indecreased conductivity values. A conversion of sodium hydroxide X ~ 0.727; and rate constant k ~ 1.27×10^{-3} m^3/mol.sec were obtained under steady state conditions.

3.2 Reactant Flow Rate

Influence of the flow rates of NaOH and CH3COOC2H5 on the conversion and rate constant were investigated. Three different feed flow rates (i.e. 6.67x10-7 m3/sec, 8.33x10-7 m3/sec and 10.0x10-7 m3/sec) were selected to analyze the reaction performance and the experiments were conducted at a fixed temperature of 30°C. Actual-time conductivity data were collected with the different flow rates. Fig.3 shows the variation of conductivity and conversion with various reactant flow rates.

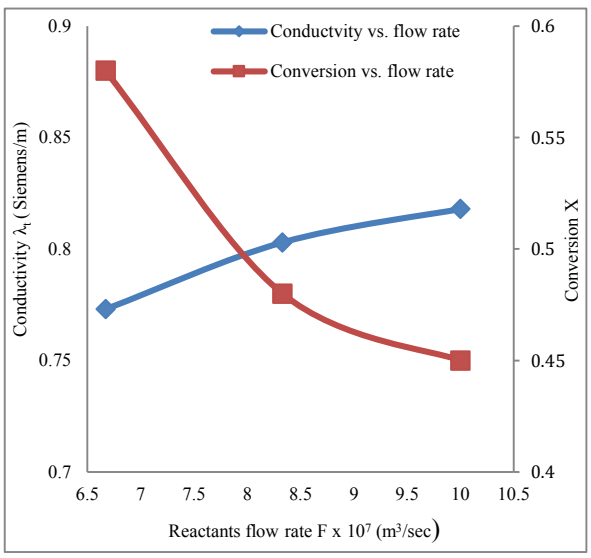

Fig.3: Effect of reactant flow rates on conductivity and conversion

The conductivity increases with reactant flow rate upto 0.818 Siemens/m at flow rates of both reactants equal to $10.0x10^{-7}$ m^3/sec as compared with 0.773 Siemens/m at a flow rate of $6.67x10^{-7}$ m^3/sec. A decrease of conductivity with an increased feed flow rate signifies the formation of less desired products. The conversion curve shows a decline with increased flow rate. Conversion reaches a value of X~ 45% at a flow rate of $10.0x10^{-7}$ m^3/sec in comparison with a value of X~ 58 % at a flow rate of $6.67x10^{-7}$ m^3/sec.

Residence time decreases with increased reactant flow rate and reaches a value of 205 sec at a flow rate of $10.0x10^{-7}$ m^3/sec of both sodium hydroxide and ethyl acetate, as shown in Fig.4. As flow rates of reactants are increased, residence time decreases, resulting in decreased conversion value. Thus higher reactants flow rates are not always desirable for practical application.

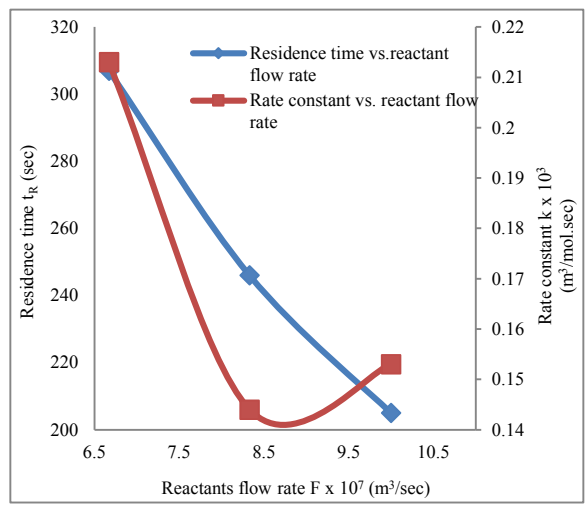

Fig. 4: Variation of residence time and rate constant with reactants flow rate

3.3 Temperature

The experiment was conducted at a flow rate of $10.0x10^{-7}$ m^3/sec for both reactants i.e., NaOH and $CH_3COOC_2H_5$. Concentration of both reactants was adjusted equal to 0.1 M NaOH and 0.1 M $CH_3COOC_2H_5$. Variation of rate constant and conversion with temperature is shown in Figure 5. It is found that the reaction conversion is a strong function of

reaction temperature, and variation is almost linear.

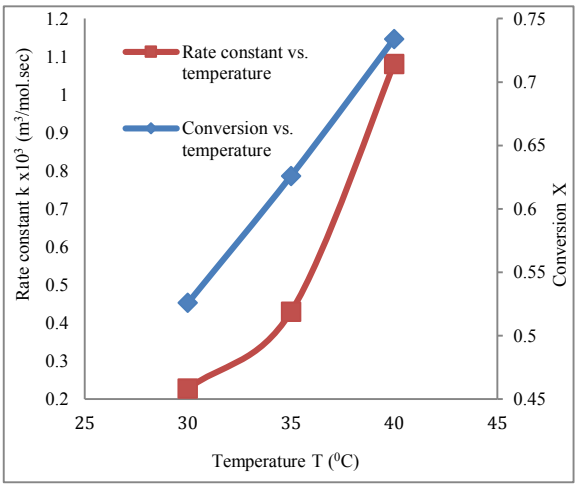

Fig.5: Rate constant and conversion versus temperature curves

Conversion varies from 52.6% at a temperature of 30 ˚C to 73.4% at a temperature of 40 ˚C. The rate constant of the saponification reaction increased from 0.228×10^{-3} m^3/mol.sec to 1.081×10^{-3} m^3/mol.sec with an increased temperature from 30 ˚C to 40 ˚C respectively. The change in conversion with temperature is more profound than the change with specific rate constant.

The results obtained at different temperatures of reaction mixture have been compared with findings reported by Wijayarathne et al. 2014 as shown in Fig. 6. Results reported by Wijayarathne et al. 2014 were obtained under a flow rate of 6.67×10^{-7} m^3/s with a reactor volume of 0.44×10^{-3} m^3. The NaOH conversion reported by Wijayarathne et al. 2014 is higher (80 % at 40 ºC) compared with the value obtained in present study (73.4 % at 40 ºC) and it may be due to the large volume of reaction mixture and lower reactant flow rate compared with. Residence time increases with decreased flow rate and this leads to increased reaction conversion.

The effect of reaction mixture temperatures on reactor performance have not been explored by the researchers (Ahmed et al. 2013) although it was suggested that conversion increases with increased temperatures of reaction mixtures (Ullah et al., 2015; Wijayarathne et al., 2014).

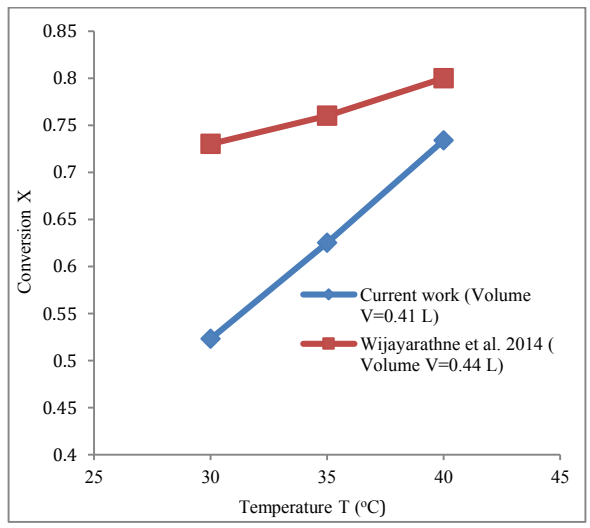

Fig.6: Comparison of NaOH conversion at different temperatures of reaction mixture with literature data (Wijayarathne et al. 2014)

4. Conclusions

In this investigation, hydrolysis of ethyl acetate (~0.1 M) with sodium hydroxide (~0.1 M) has been studied. The advancement of the saponification reaction was observed by monitoring conductivity data under different process conditions. Sodium hydroxide and sodium acetate impart conductance to the

hydrolysis reaction. Experiments were performed at a pressure of 1 atmosphere (atm) and a concentration of 0.1 M of both reactants. The influence of operating conditions such as reactant flow rate, residence time, and temperature on conversion and specific rate constant has been analyzed. The research outcomes may be outlines as follows:

- Decline in the value of actual time conductivity with time signifies the progress of the hydrolysis reaction.
- A steady-state conversion value of 72.7% and specific rate constant equal to 1.27x10-3 m3/mol.sec were achieved after time interval of 30 minutes.
- The reaction conversion diminishes with an increased reactant flow rate; this is due to the decrease of residence time.
- On the other hand, the rate constant first decreases and then increases within the studied range of reactant flow rates.
- Conversion increases almost linearly with temperature, from 0.526 to 0.734 for a temperature change from 30°C to 40°C. The maximum factional conversion of 0.734 was achieved at a temperature of 40 oC under studied range of temperatures.
- The specific rate constant also increases with increased temperature but not as profoundly as does conversion.

Acknowledgement

The authors are thankful for the support of the laboratory staff at King Khalid University, Abha KSA.

Nomenclature

M	Reactants concentration	mol/liter
V	Volume of reactor	m^3
F	Reactant flow rate	m^3/sec
X	Reaction conversion	(-)
t_R	Residence time	sec
k	Rate constant	m^3/mol.sec
T	Temperature	^oC
t	Time	sec

Greek Symbols

λ	Conductivity	Siemens/m

References

Ahmad, A., Ahmad, M.I., Younas, M., Khan, H., Shah, M.H., 2013. A Comparative Study of Alkaline Hydrolysis of Ethyl Acetate using Design of Experiment. Iran. J. Chem. Chem. Eng. 32(4), pp.33-47.

Bursali, N., Ertunc, S., Akay. B., 2006. Process Improvement Approach to Saponification Reaction Using Statistical Experimental Design. Chem. Eng. and Process 45, pp. 980-989.

Daniels, F., Mattews, J., Williams, J., 1941. Experimental Physical Chemistry, McGraw–Hill, New York.

Danish, M., Al Mesfer, M.K., Rashid, M.M., 2015. Effect of Operating Conditions on CSTR Performance: an Experimental Study, Int. J. Eng. Res. Appl. 5, pp.74-78.

Fogler, H.S., 2006. Elements of Chemical Reaction Engineering, 4th Ed., Pearson Education Inc., New Jersey.

Kapoor, K.L., 2004. A Textbook of Physical

Chemistry, McMillan India Ltd., New Delhi.

Kuheli.D., Sahoo. P., Saibaba. M., Murali. N, Swaminathan. P., 2011. Kinetic Studies on Saponification of Ethyl Acetate Using an Innovative Conductivity –Monitoring Instrument with a Pulsating Sensor,Int. J. Chem. Kinet 43, pp. 648-656.

Grau, M.D., Nougues, J.M., Puigjaner, L., 2002. Comparative Study of two Chemical Reactions with Different Behavior in Batch and Semibatch Reactors, Chem. Eng. J. 88, pp. 225-232.

Schneider, M.A., F. Stoessel., 2005. Determination of Kinetic Parameters of Fast Exothermic Reactions, Chem. Eng. J.115, pp.73-83.

Tsujikawa, H., Inoue, H., 1966. The Reaction Rate of the Alkaline Hydrolysis of Ethyl Acetate, Bull. Chem. Soc. Jpn. pp. 1966-1842.

Ullah, I., Ahmad, M.I., Younas, M., 2015. Optimization of Saponification Reaction in a Continuous Stirred Tank Reactor (CSTR) using Design of Experiments, Pak. J. Engg. & Appl. Sci. 16, pp. 84-92.

Wijayarthne, U.P.L., Wasalathilake, K.C., 2014. Aspen Plus Simulation of Saponification of Ethyl Acetate in the Presence of Sodium Hydroxide in a Plug Flow Reactor, Int. J. Chem. Nucl. Metall. Mater. Eng.8, 992-999.

Walker, J., 1906. A Method for determining velocities of Saponification, Proc. R. Soc. Lond. A 78, pp.157-160.

Development of a Polymer Modified Flexible Pavement Material for Sustainable Pavement System

Sami A. Osman*
Assistant Professor, Department of Transportation Engineering College of Engineering, University of Dammam, Kingdom of Saudi Arabia,
sakhair@uod.edu.sa

Muhammad Saleem
Associate Professor, Department of Basic Engineering, College of Engineering, University of Dammam, Kingdom of Saudi Arabia, mssharif@uod.edu.sa

Rana Sajid Khan
Lecturer, Department of Transportation Engineering, College of Engineering, University of Dammam, Kingdom of Saudi Arabia,
rmSajid@uod.edu.sa

Muhamad Abid
Lecturer, Basic Engineering Department, College of Engineering, University of Dammam, Kingdom of Saudi Arabia,
maakhan@uod.edu.sa

Abstract
In Kingdom of Saudi Arabia (KSA) number of vehicles increased dramatically with an annual growth rate of 5 to 6%. This increase in number of vehicles lead to heavy traffic loads which lead to structural problems for the layer of the pavement. There has been a huge amount of investment in road infrastructure. Accordingly, road network is facing different problems in different aspects such as bituminous materials, loading and design method. A detailed experimentation has been carried out to investigate and evaluate the binder, aggregate and mixture composition, air void, materials characterization and improving pavement performance by using five different types of polymers with different concentrations. Several mixes were tested using Marshal tests. Dynamic shear Rheometer used to characterize bitumen and modified bitumen. Results show that use of plastomer polymers types (e.g. Polybilt-101, EE2) to modify the asphalt binder by improving their physical and rheological properties to meet the performance requirements is effective. It is possible to use different types of polymers (LDPE and HDPE) and different percentage of polymer concentration to achieve the performance requirements (e.g. PG 70 can be achieved by using 3% of EE2 or 4% of Polybilt).. It can concluded that the asphalt 60/70 pen grade which is used today in eastern province, KSA, meets the performance requirements to resist the main distress of flexible pavement. The asphalt binder behavior affects the performance of asphaltic concrete mixes. However, there are several important characteristics of asphalt binder (e.g. the adhesion of .asphalt binder to aggregate) should be evaluated besides modification of asphalt binders

.**Keywords**: Asphalt;asphalt mixture; polymers; modified asphalt

1. Introduction

Cracking in road can occurs at an intermediate and low temperatures, and permanent deformation can occurs at high temperatures. These are the most serious distresses for the flexible pavements. These

distresses are reducing the pavement life; in addition to increasing maintenance cost (KACST, 1993). Permanent deformation is important type of distresses and the principle class of this type is rutting. Rutting occurs in the flexible pavements when vehicles loads cause shear stresses which are more than the shear strength of the materials used to construct the pavement so that it depends on the vehicular loads and the visco-elastic properties of the bitumen. This means bitumens are required to have high stiffness at high temperature to resist rutting. The bitumen behavior affects by its chemical composition. The atoms in molecules and its type of structures are the affecting factors to the bitumen behavior, therefore, it is more necessary than the total amount of each element. On the other hand, the study of chemical properties is more complicated, this is why the physical and rheological properties are used to characterize the asphalt binder because they are easy to understand in addition, they give indication about the chemical components (http://www. new-technologies.org, 2016). The fast increase in the number of vehicles in KSA and associated loads lead to development of different problems to the layered structure of the pavement. This means the existing design approaches need to be reviewed for effectiveness specifically the methods which depend on empirical analysis of loads. The performance of flexible pavement affected mainly as material properties, vehicles loads, environment and methods of construction. Most of the design methods based on the field tests and experience gained from the American Association of State Highway Officials (AASHTO). The new approaches for the pavement design are based on the analysis of stresses and strains or deflection to calculate the permanent deformation and pavement fatigues using multilayers system (AASHTO, 2010). The tensile strains under the bituminous layers can leading to fatigue cracking and rutting due to strain at top of subgrade layer. Saeed and Ali explore the uses of fibers in asphalt mixtures. They said that use of fibers as an additives materials is not a new phenomenon, bitumen-fiber material have been used since 1950. Today in developed countries most of concrete used in construction industry are improved by additives (Saeed et al., 2008). Extensive research works are undergoing using different fibers and asphalt binder (Vikas and Shweta, 2006; Hossam et al. 2005). It can be concluded that they affect the performance of asphalt mixes. Any addition of fiber can lead to significant changes to mixture properties, even more investigation and experimental works are required to prove their effects (Pyeong et al. 2010). Extensive research has been conducted or in progress all over the world including costly accelerated dynamic field testing to replace or modernize the existing conventional design methods. The dynamic-response parameters are needed as fundamental inputs to modern evaluation and mechanistic design of pavements. These properties will also allow characterization and comparative

studies of available conventional, marginal and treated highway materials. The results of laboratory test, related with the theoretical predictions, will permit comparison with actual pavement performance available from field measurements. The findings from such studies will ultimately lead to adoption and use of new or improved materials based on satisfactory performance (Preston, 1997).

Fatigue of mixtures can be assessed reasonably satisfactorily in a number of ways and such tests are now routinely carried out in many countries as part of a mixture design process. However, the relative importance of the different mixture components is not well understood, nor is the real relationship between fatigue in laboratory tests and that in the road pavement. Currently several factors, such as temperature and moisture are considered in the different modeling techniques applied for paving mixtures and flexible pavements. However, in regions where hot climate prevails, like in KSA, the following two main factors ought to be accounted for when investigating for the permanent deformation and fatigue cracking:

a. Environmental effects, basically high temperature during most of the year, and

b. Use of the materials available in the project area.

The primary methods of modeling and analysis include elastic, viscoelsticity, elasto-plasticity, visco-plasticity and finite element. The most important parameters used in these analytical methods are the resilient modulus and the complex modulus (Qi and Witczak, 1998). Asphalt binder is complex materials due to heterogeneous structure. Many researches carried out worldwide to understand its behavior. Recently research works carrying out to simulate fatigue cracking and permanent deformation through models of materials [Lee et al. 2000; Lytton, 1993; and Park, 1996). There is an obvious difference between the relatively uniform stress conditions present in a pure binder specimen and the highly variable stresses present in the binder around numerous filler particles. The analysis demands innovative thinking (Osman, 2005). Permanent deformation or rutting and fatigue cracking are the main distresses facing the flexible pavement. Polymer modification has been proven to be an effective way to improve bitumen properties to some extent by many researchers and has been used widely in practice (Nahal et al 2014, Zhu et al 2014)

Abdulaziz**,** 2001 conducted a research that stated; that the fatigue cracking and rutting in the shape of longitudinal depression are the main distresses in KSA in spite other failure modes. Due to heavily trucked highways and overweight of trucks pressure of tire rutting is almost the dominant distresses in Eastern province. So to overcome these problems asphalt mixture materials, design and method of construction should be changed to obtain high quality pavement (Abdulaziz, 2001). Some researchers have found that adding polymers to asphalt may increase the product price by between 60 and 100% owing to following reasons (Al-Dubeeb et al. 1998).

Price of polymer and content of polymer can decrease, Pavement cycle cost increase by 10 folds, Most used polymer in asphalt modification is Styrene ButyleStyrene and crumbed tire rubber. Fig. 3 shows temperature zoning map and performance Grade (PG) binder That can be used in Kingdom of Saudi Arab.

2. Materials and Methods

Asphalt grade 60/70 Pen was used in this research collected from Ras-Tanora refinery. Fifty liters of asphalt were collected and distributed into small containers after heating to avoid repeating of heating samples which may change the characteristics of asphalt binder. Polymers samples were collected from three sources: SABIC polymers: two types of High Density Polyethylene (HDPE); HDPE M80064 and HDPE M200056, one type of Linear Low Density Polyethylene (LDPE), Exxon Chemical (EE2) and Eastman Polybilt Polymer (PB-101).

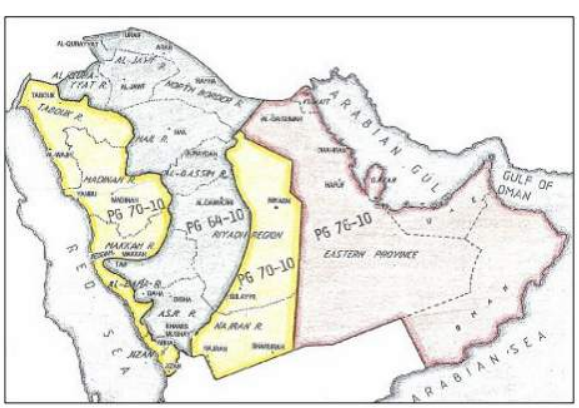

Fig. 1. Temperature Zoning Map and binder PG for the Kingdom of Saudi Arabia (Hamad, 1996).

2.1 Preparation of polymer and asphalt blend

Five polymers were used in this research, individual polymer blended with asphalt grade 60/70 Pen. To insure homogeneity of the product the heating temperature and blending time had been followed as per manufacture's recommendation. Of course experience playing a major role in defining the polymer concentration of the selected types. The specified percentage of each polymer was used to produce the Polymer Modified Bitumen. Aggregate from different sizes were blended by trial and error to achieve the aggregate skeleton as per specifications (MOM &RA – KSA, 2011). Marshal mixture design was used to evaluate the asphalt mixture. Aggregate mixture was heated to160-180°C. Bitumen also heated to 170°C.

2.2 Asphalt Mixture Design

Asphalt mix is designed using different polymers types. A control mix was designed using the specifications of Ministry of Transport in Eastern Province. Asphalt mixes sample were prepared (see Fig. 2):

Fig. 2.Samples of control mix, mix1

Mix 1: Control mix as used in eastern province specifications, KSA without using asphalt modifier 3 samples per bitumen content by weight has been used.

Mix 2: Modified Asphalt with HDPE M80064 polymer 3 samples per bitumen content.

Mix 3: Modified Asphalt with LLDPE M200024 polymer 5 samples with bitumen content.

Mix 4: Modified Asphalt with HDPE Polybilt polymer 5 samples with bitumen content.

Mix 5: Modified Asphalt with HDPE EE2 polymer 5 samples with bitumen content.

3. Results and Discussions

3.1 Aggregate Testing Results

Aggregate is a mix of granular particles with different sizes and shapes produced by mechanical crushing of natural or industrial stones. Samples of coarse and fine crushed aggregates materials were obtained from Abu Mean company. Cement filler was used in asphalt mixture as a filler material. Coarse aggregates were evaluated using different methods such as: abrasion test, impact value, crushing value, gradation, water absorption and specific gravity, angularity, flakiness index and elongation. Finer materials were evaluated by using sieve analyses, specific gravity and absorption. Table 1 presents the specific gravity and other properties of the aggregate samples. Table 1 presents the results of physical properties of the asphaltic materials.

3.2 Testing of Asphalt Binders

The total numbers of asphalt binders tested are five including the neat (un-aged) asphalt binder 60/70 pen grade and four modified binder. Two percentages of polymer contents for each types is used to achieve different PG grades. Series of testing was established to get the physical and consistency properties

Table 1. Properties of aggregate used in asphaltic concrete

Test	Test used	Aggregate size			
		3/4"	3/8"	Crushed sand	Filler
Magnesium Sulphate soundness loss, %	ASTM C88-05	10	10	11	-
Los Angles Abrasion Value, %	AASHTO T-96 ASTM C 131	29.2	29.5	-	-
Aggregate Impact Value	BS 812-112	11.2	11.2	-	-
Specific gravity for Bulk	AASHTO T85	2.572	2.25	2.636	2.673
Specific gravity for Saturated Surface Dry		2.627	2.28	2.684	
Apparent Specific Gravity		2.72	2.34	2.777	
Absorption of Water, %		2.1	1.74	2.0	-
Flakiness index,%	ASTM D4791-05	4.8	31	-	-
Elongation index,%	ASTM D4791-05	2.5	21.3	-	-
Clay content, %	AASHTO T-112	0.20		0.17	
Coating and stripping, %, min.	AASHTO T-182	95			
Liquid Limit	ASTM D4318	-	-	N.L	N.L
Plastic Limit	ASTM D4318	-	-	N.P	N.P

in the laboratory as shown in Table 2. For each test, four samples were experimented to eliminate the percentage of error. Table 3 gives summary of binder characterization test results. Asphalt binder properties evaluated through superpave tests corresponding to different temperature range like low, medium and high as shown in Table 3. Dynamic Shear Rheometer (DSR) AASHTO TP-5 is used for properties determination at intermediate and high temperatures to evaluate both neat and modified asphalt.

The (DSR) test conducted to determine the rheological properties for aged and un-aged asphalt binder samples. The DSR test provides different parameters - at a temperature range from 22 to 40°C, and for flexural creep between -6 to -12°C as shown in table 3- as listed below:

- Complex Shear Modulus, G* = Peak Stress / Peak Strain
- Phase Angle, d (defined as the phase difference between stress and strain)
- Shear Storage Modulus, G′ = G* Cos δ
- Shear Loss Modulus, G″ = G* sin δ
- G* / sin δ

The established sequenced is followed to determine the PG grade of asphalt binder samples. Bending Beam Rheometer (BBR) test is used for the low temperature properties (creep stiffness (S) and creep

Table 2. Bitumen Physical Properties Tests Results

Property	AASHTO Test	Penetra-tion Grade 60-70	Mean test value
Penetration at 25 Degrees C, 100g, 5sec.	T-49	68	2.21
Viscosity, at 60 °C, Poise,	T-202	2750	0.96
Flash point, Cleveland Open, °C,	T-48	235	0.82
Fire point, Cleveland Open, °C,.	T-48	245	0.817
Ductility at 25 °C, 5cm per min, cm,	T-51	104	
Solubility in trichloroethylene, percent,	T-44	99	
Specific gravity		1.03	0.002
Softening Point (˚C)		49.3	0.153

Table 3.Summary of Polymer Binder Characterization Results.

Tests	Grade 60/70	EE2 4%	EE2 5%	PB 4%	PB 5%
Viscosity (cP) (RV) max 3000Cp	494.25	450	425	450	837.5
Mass Loss % (RTFO) max 1%	(+) 0.344	(-) 0.037	(-) 0.034	(-) 0.01	(+) 0.020
G*/Sinδ (OB) (DSR) ≥1kPa	1.343	1.302	1.460	1.828	1.801
G*/Sinδ (RTFO) (DSR) ≥2.2kPa	3.384	2.673	3.614	3.620	3.282
G*Sinδ (PAV) (DSR)<5MPa	4.386	3.994	3.097	1.811	1.486
Stiffness (BBR)<300 MPa	167	182.5	187	102.1	50.7
m-value (BBR)≥ 0.30	0.345	0.325	0.314	0.33	0.307
PG	64-22	70-22	76-22	70-16	76-16

rate (m-value)) evaluation. Pressure Aging Vessel (PAV) (AASHTO PP-1) residue are the samples used for BBR test for both neat and modified asphalt binder. As a definition the creep rate is the slope of log loading time versus log stiffness. The Rotational Viscosity test at 135ºC performed using Rotational viscometer (RV AASHTO TP-48) is a valuable conducting test to evaluate the workability, pumping and handling for both types of binder (neat and modified). One advantage of the RV test is that the result could be used to determine the mixing and compaction temperatures based on temperature versus viscosity chart by testing the viscosity at 163 ºC. The Rolling Thin Film Oven (RTFO, ASTM D-2982) and PAV method were used to simulate the short and long term aging respectively for modified and un-modified (60/70 pen grade) asphalt binders samples. There was no need to conduct the Direct Tension Test (DDT) because of the BBR test results.

3.3 Asphalt Mixture Results

Fig. 3 to Fig 7 shows asphalt mixture properties for Marshall testing.

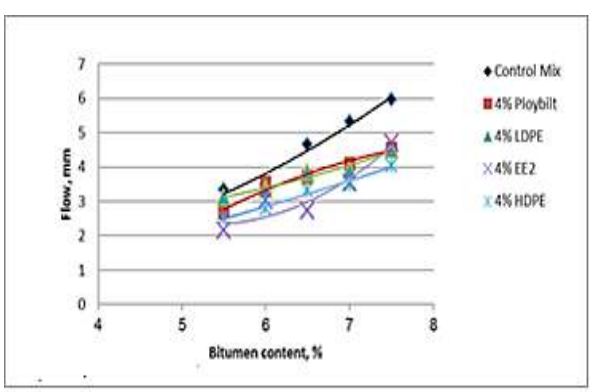

Fig.3. Bitumen contents Vs. mix stability

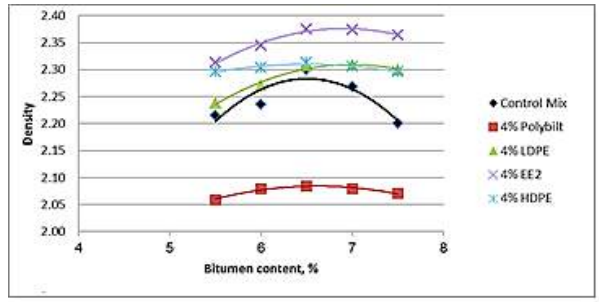

Fig. 4. Bitumen contents Vs mix density(kg/m^3)

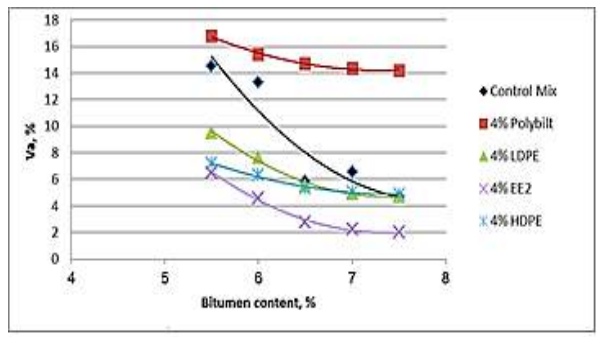

Fig. 5. Bitumen contents Vs air voids

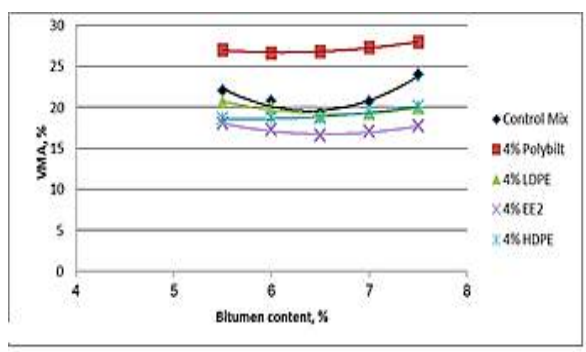

Fig. 6. Bitumen contents Vs Voids in mineral aggregate

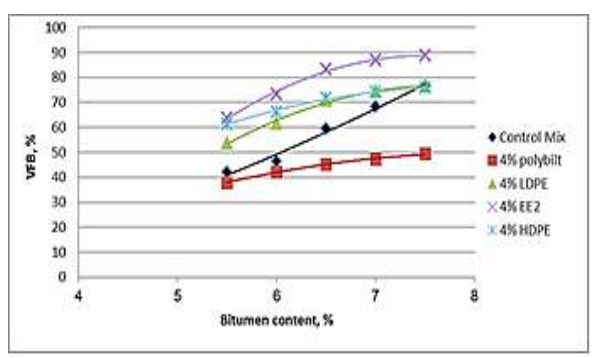

Fig. 7. Bitumen contents vs Voids filled with bitumen

3.4 Discussion

AASHTO specifications are used for sample preparation and polymer blend with provided recommendations by the manufacturer. Appropriate percentage selection of the polymer was a considerable point and this selection of the previous percentage of polymers contents based on the experience. Bitumen binder is a visco-elastic material and its properties affected by two factors - which are load time and temperature - extensive evaluation had been done using Superpave tests methods and PG grade system. The PG grade was determined to see whether it satisfies the specification requirements according to the Temperature Zoning in KSA as shown in Fig. 3 above. So that, resistance to rutting and fatigue cracking was covered. In addition to that workability, safety, pumping and handling characteristics are evaluated.

Based on SHRP Superpave System the performance of asphalt binders in specified location is controlled by two factors, these are: the average seven day maximum pavement design temperature and the minimum pavement design temperature. As a result of the research, the temperature zoning of KSA which is shown in Figure 3 are identified (-10 ºC) as the minimum pavement design temperature and (70 ºC) as the maximum pavement design temperature, but the asphalt binder samples which are collected from the refinery had the minimum required G*/sin (δ) which is 1.0 KPa at 64ºC. So that, the produced asphalt binder from the refinery do not meet the performance requirements of more than 60% of KSA area. So this type of asphalt (60/70 pen Grade) can be used without modification in some locations, if the traffic condition does not require developing of PG based on Table 3, otherwise modification is required. For the other areas asphalt modification is needed to improve asphalt binder properties to satisfy the required PG grade, because 60/70 pen grade asphalt do not exhibit adequate visco-elastic properties to resist high temperature distresses in areas when the high pavement design temperature exceed 64 ºC. In this regard, two types of polymers from international producer used to modify the 60/70 pen grade asphalt binder samples from the refinery. Modification of asphalt does not mean to check the requirements at high temperature only, so that, it is important to note that, although the performance of low temperature requirement of asphalt binder in KSA (-10 ºC) is satisfied by 60/70 pen grade asphalt binder, the polymer modified binders must be evaluated for their low temperature behavior to insure that the modification does not affect their behavior at low temperatures as a tradeoff for the improvement of their behavior at high temperatures.

According to the laboratory results which were shown in Table 3 it is evident that the PG 76 could be achieved by using the same percentage of the two different types of polymers (5%) but, the low temperature is different. On the other hand, the PG 70 can be achieved by using 4% of EE2 or 4% of Polybilt. It is important to note that, the

rheological properties of modified bitumen binder using two or more different types of polymers were not depending on the percentage of polymers, even they gave same high temperature properties requirement at one percent.

On the basis of the asphalt mixture results obtained, comparison can be establish in the optimum asphalt content between the control mix and the modified polymers as following:

- Target optimum asphalt content for HDPE M200056 polymer is less than Control mix
- Target optimum asphalt content for LLDPE M200024 polymer is less than Control mix
- Target optimum asphalt content for Polybilt polymer is less than Control mix
- Target optimum asphalt content for EE2 polymer is less than Control mix

4. Conclusion

Based on the above Marshal design results the following points can be concluded:

- Mixture Flow of unmodified asphalt is higher compared with all modified asphalt. Lower value of flow obtained when using EE2 polymer and HDPE.
- Low stability was obtained from unmodified mixture whereas high stability was obtained when using EE2 and HDPE polymers. Polybilt modified mixture gave lower stability compared with other modified polymers.
- EE2 modified mixture gave a higher density compared with other mixes. But a polybilt mixture gave low density than the control mix.
- Polybilt mixture gave high air voids content even higher than the control mix. The others modifiers gave lower air voids compared with control mix. Similar results were obtained for voids in mix aggregate (VMA).
- As a consequence the polybilt mixture gave lower voids filled with bitumen compared with other modifiers.
- Based on the testing results and analysis, for modified and un-modified asphalt binder, the following conclusion can be stated:
- The asphalt 60/70 Pen grade which is used today in Eastern province, KSA, meets the performance requirements to resist the main distress of flexible pavement (Fatigue cracking and permanent deformation), where the maximum temperature of pavement at the specified depth does not exceed (70 ºC) and the minimum temperature of pavement is not below (-10 ºC).
- Use of plastomer polymers types (e.g. Polybilt-101, EE2) to modify the asphalt binder by improving their physical and rheological properties to meet the performance requirements is effective.
- It is possible to use different types of polymers and different percentage of

polymer concentration to achieve the performance requirements (e.g. PG 70 can be achieved by using 3% of EE2 or 4% of Polybilt).

- The concentration and type of polymer affect the rheological properties and workability of modified asphalt binder.
- Blending and mixing of polymers produces a homogenous mix with complete dispersion within the body of asphalt binder.
- The plastomer types of polymers are easiest in processing of asphalt blend because it does not need high shear mixer and some types (e.g. Polybilt-101) can be added directly in the asphalt plant during the production of asphalt mixes.
-

Acknowledgment

The author is grateful to the Deanship of Scientific Research (DSR) at the University of Dammam for the financial support. The publication is part of the project funded by the DSR under the project ID 2014251.

References

AASHTO., 2010. Standards American Association of State Highway and Transportation Officials. Washington, D.C. Accessed on 1st May 2016.

http://www. new-technologies.org/ECT/CIVILsuperpave.htm.

Abdulaziz, A., Bubshait., 2001. Quality of Pavement Construction in Saudi Arabia, Practice Periodical on Structural Design, and Construction. 6(3), ASCE, ISSN 1084- 0680/01/0003, pp 129–136.

Al-Dubeeb, Ibrahim.,Al-Abdul, Wahab, H.I., and Asi, Ibrahim., 1998. Polymer Modification of Arab Asphalt, Journal of Materials in Civil Engineering 10(3), pp 161-167.

Hamad. Al-Al-Abdlwahab, M. Farahat Ali, Ibrahim A. Al-Dubabe., Ibrahim M. Asi., 1996. Adaptation of SHRP Performance-Based Asphalt Specification to the Gulf Countries, Final Report, King Abdul Aziz City for Science and Technology (KACST).

Hossam, F., Hassan, Salim Al-Oraimi., Ramzi, Taha., 2005. Evaluation of Open-Graded Friction Course Mixtures Containing Cellulose Fibers and Styrene Butadiene Rubber Polymer, Journal of materials in civil engineering 17(4), pp 416-422.

King Abdulaziz City for Science and Technology (KACST)., 1993. Adaptation of SHRP Performance Based Specification to the Gulf Countries, research project (https://www.kacst.edu.sa/eng/Pages/default.aspx)

Lee, H. J., J. S. Daniel., Y. R. Kim., 2000. Continuum damage mechanics based fatigue model of asphalt concrete, Journal of Materials in Civil Engineering 12(2), pp 105-112.

Lytton, R., J. Uzan., E. G. Fernando., R. Roque., D. Hiltunen., 1993. Development and validation of performance prediction models and specifications for asphalt binders and paving mixes. The Strategic Highway Research Program Report

SHRP-A-357, National Research Council, Washington D.C.

Ministry of Municipal & Rural Affairs – Kingdom of Saudi Arabia. 2011. General Specifications of Urban Roads, Construction Division 7- Materials of Asphaltic Mixes.

Nahla Yassoub Ahmed Ahmed Sundus Mohammed AL-Harbi, 2014' Effect of Density of the Polyethylene Polymer on the Asphalt Mixtures, Journal of Babylon University/Engineering Sciences/ No.(4)/ Vol.(22), pp674-683

Osman, S.A., 2005. The role of bitumen and bitumen filler mortar in asphalt mixture fatigue, PhD thesis, Nottingham University, UK.

Park, S. W. A., 1996. Viscoelastic continuum damage model and its application to uniaxial behavior of asphalt concrete, Mechanics of Materials 4, pp 241 -255.

Pyeong, J. Y., Ji Young, Choi., Byung-Sik, Ohm., 2010. Characteristics of Mono-Strand Fiber-Reinforced Hot-Mix Asphalt Mixtures, ASCE, pp 449-461.

Preston, N., 1997. Analytical Pavement Design, Highways and Transportation, UK, 44(12), pp 15-19.

Qi, X., Witczak, M.W., 1998. Time-Dependent Permanent Deformation Models for Asphaltic Mixtures, Transportation Research Record No. 1639, Transportation Research Board, Washington, D.C. pp 83-93.

Saeed, J., Khodaii, 2008. Carbon Fiber Reinforced Asphalt Concrete, The Arabian Journal for Science and Engineering 33(2B), pp 355-364.

Vikas, Sharma, Shweta, Gpyal., 2006. Comparative study of performance of natural fibers and crumb rubber modified stone matrix asphalt mixtures, Canadian Journal of Civil Engineering, 33(2), pp 134-139.

Zhu, J., Birgisson, B., Kringos, N.; 2014; Polymer modification of bitumen: Advances and challenges, European Polymer Journal, 54: 18-38, http://dx.doi.org/10.1016/j.eurpolymj.2014.02.005

Non-uniform Incident Illumination Effect on the Thermal Performance of Low Concentrating Multi-Junction Solar Cells

Fahad G. Al-Amri
Department of Basic Engineering, College of Engineering, University of Dammam, P.O. Box 1982, Dammam 31441, Saudi Arabia, fgalamri@uod.edu.sa

Abstract

The modern multi-junction concentrating solar cell is an emerging technology that is expected to play a crucial role in achieving solutions to energic and environmental challenges that the world faces today. A potential technical limit to widespread adoption of this technology is the degradation of solar cell efficiency at high operating temperatures. In this paper, a numerical heat transfer model is presented and applied to determine the effects of non-uniform incident illumination on the operating temperature of a triple-junction solar cell. Results show that even at quite low solar concentrations, maximum solar cell temperature significantly increased in the presence of non-uniform incident light, causing hot spots in some portions of the cell. Thus, a conventional cooling system, such as a plain channel, is insufficient for operating solar cells at reasonable temperatures under non-uniform illumination. However, the non-uniformity of the incident radiation has no effect on bulk fluid temperature and collected thermal energy at the duct exit.

Keywords: Concentration solar cell; non-uniform illumination profile; active cooling; conjugate convection; surface radiation

1. Introduction

The incident light on the surface of a concentrating solar cell is strongly non-uniform (Baig et al., 2012). As a result, the majority of light is intensified onto a small area of the cell surface, causing a hot spot in this part of cell. This in turn causes a current mismatch and degradation in the overall efficiency of the CPV. Several researchers have investigated the effect of non-uniform incident light on electrical performance (Franklin and Conventry, 2003), but few have studied the thermal impact of the problem. The experimental study by Conventry et al. (2002) showed that a silicon solar cell under non-uniform incident illumination has less open-circuit voltage and efficiency compared to a cell under uniform light. Domenech-Garret (2011) explored the influences of a combination of non-uniform illumination and non-uniform temperature on a silicon solar cell. Gaussian and inverse Gaussian profiles were used to describe the temperature in the cell, which simulated a general cell cooling device. Chemisana and Rosell (2011) investigated, both numerically

and experimentally, the effects of Gaussian and anti-Gaussian temperature profiles on the electrical performance of the cell under various types of concentrated radiation. They found that electric conversion efficiency increases under a Gaussian temperature profile and decreases when the cell is subjected to an inverse Gaussian temperature curve. They concluded that the temperature profile could be tailored to maximize efficiency under determined radiation conditions. Al-Amri and Mallick (2014) investigated the combined effects of surface radiation and forced convection on the concentrating triple-junction solar cell temperature under non-uniform illumination and at medium solar concentration. They found that surface radiation exchanged inside the channel reduced cell temperature. Recently, Xing et al. (2016) studied the electrical and thermal performances of a silicon triple-junction solar cell under non-uniform light. As the degree of non-uniformity increased, a remarkable increment in cell temperature was observed.

It is well observed and documented in the literature that the cooling of PV panels increase the electrical efficiency of such systems. Presently several PV cooling methodologies exist that include active water and air cooling and passive techniques such as PCM cooling, conductive cooling, etc (Kumar & Rosen, 2011). The passive cooling techniques have an advantage of using natural means to provide cooling yet such systems are comparatively larger in size, need higher capital investment and have complex maintenance. This limits the applicability of passive cooling system. On the contrary, plain channel air/water cooling is still far better than the others because of its simplicity, smaller size, less capital investment and easy maintenance although they require electrical input for continuous operation (Grubisic-Cabo et al. 2016).

To the best of our knowledge, at low solar concentrations, the non-uniformity effect of the incident light has not been investigated. Therefore, in this study, a numerical model was developed to determine the temperature distribution on the low concentrating solar cells under non-uniform incident illumination. The results of this work will aid estimation of the overall efficiency of a CPV system and assessment of the adequacy of a conventional cooling system in maintaining cell temperatures below the acceptable limit.

2. Mathematical Formulations

The triple-junction solar cell employed in this work consisted of three semiconducting materials, galium indium phosphide (GaInP), galium arsenide (GaAs), and germanium (Ge), each absorbing a different spectrum of incident light, and a front contact, Cu-Ag-Hg, for capturing the generated current. It was attached to a front cover glass and a rear aluminum duct via adhesives (see Figure 1). The properties and dimensions of these components can be found elsewhere (Al-Amri and Mallick, 2013). The duct walls were considered to be gray, opaque, and diffuse surfaces, and the inlet and exit areas were

considered to be black surfaces. In addition, it was assumed that the external wall was adiabatic, that air flow entered at a constant velocity (u_∞), that ambient temperature was constant, that cell conversion efficiency (η) was 0.38, and that reflectivity was 0.85 for the front metal contact and zero for all other cell components. The illumination distribution incident on the concentrating cell surface was strongly non-uniform and took the shape of a Gaussian profile (Franklin and Conventry, 2003). Therefore, the formula of the light intensity adopted in the current model was:

$$I(z) = \frac{2C}{10^4\ SD\sqrt{2\pi}}\, e^{\frac{-2(z-z_0)^2}{S^2}} \qquad (1),$$

where z_0 is the position of the maximum illumination on the cell surface, and S is the standard deviation of the illumination, measuring how far the illumination is spread out.

The intensity of incident light I(z) can be written in the non-dimensional form as:

$$\bar{I}(Z) = \frac{I(z)}{I_{avg}} \qquad (2),$$

where I_{avg} is the average incident illumination across the entire cell surface.

The physical problem under consideration is governed by the energy conservation equation in solid regions and the equations of energy, continuity, and momentum in fluid regions under the constraint of radiation equations along each of the two channel walls. These equations can be written under usual boundary assumptions (Al-Amri and Mallick, 2013).

Continuity equation

$$\frac{\partial V}{\partial Y} + \frac{\partial U}{\partial Z} = 0 \qquad (2)$$

Momentum equation

$$V\frac{\partial U}{\partial Y} + U\frac{\partial U}{\partial Z} = \frac{dP}{dZ} + \frac{G_r^*}{Re}(\theta - \theta_\infty) + \frac{\partial^2 U}{\partial Y^2} \qquad (3)$$

Energy equation fluids

$$V\frac{\partial \theta_f}{\partial Y} + U\frac{\partial \theta_f}{\partial Z} = \frac{1}{Pr}\ \frac{\partial^2 \theta_f}{\partial Y^2} \qquad (4)$$

Energy equation for each solid material

$$\frac{\partial^2 \theta_s}{\partial Y^2} = 0 \qquad (5)$$

The integral form of the continuity equation was also utilized to solve the problem (Al-Amri, 2008; Al-Amri and El-Shaarawi, 2010):

$$F = \int_0^1 U dY = 1 \qquad (6)$$

The surface radiation exchanges inside the channel are determined by applying the first law of thermodynamic per unit surface area on the channel plate element (Al-Amri, 2008; Al-Amri and El-Shaarawi, 2010), yielding the following two constraint equations:

Surface 1 (Y = 0)

$$N_{rad}\ \theta_\infty^4 \left[\frac{1}{2} - \left(\frac{ZRe}{2}\right)\left(1 + Z^2\ Re^2\right)^{-\frac{1}{2}}\right]$$

$$+ N_{rad}\theta_e^4 \left[\frac{1}{2} - \left(\frac{(L-Z)Re}{2}\right)\left(1 + (L-Z)^2\ Re^2\right)^{-\frac{1}{2}}\right]$$

$$+\int_0^L \left\{ \frac{1-\varepsilon_2}{\varepsilon_2} \left(\left.\frac{\partial \theta_f}{\partial Y}\right|_{Y=1^-} - \left.\frac{\partial \theta_s}{\partial Y}\right|_{Y=1^+} \right) + N_{rad}\theta_{w2}^4(Z) \right\}$$

$$\left[1+Re^2(Z-Z')^2\right]^{(-3/2)} \frac{Re}{2} dZ' = -\frac{1-\varepsilon_1}{\varepsilon_1} \left.\frac{\partial \theta_f}{\partial Y}\right|_{Y=0^+}$$

$$+ N_{rad}\,\theta_{w_1}^4(Z) - \left.\frac{\partial \theta_f}{\partial Y}\right|_{Y=0+} \qquad (7),$$

where $N_{rad} = \sigma q_{avg}^3 \frac{b^4}{k_f^4}$.

Surface 2 (Y = 1)

$$KR_{s_1-f} \left.\frac{\partial \theta_s}{\partial Y}\right|_{Y=1^+} + N_{rad}\,\theta_\infty^4 *$$

$$\left[\frac{1}{2} - \left(\frac{Z\,Re}{2}\right)\left(1+Z^2\,Re^2\right)^{-\frac{1}{2}}\right]$$

$$+ N_{rad}\,\theta_e^4 \left[\frac{1}{2} - \left(\frac{(L-Z)}{2} Re\right)\left(1+(L-Z)^2\,Re^2\right)^{-\frac{1}{2}}\right]$$

$$+\int_0^L \left\{ \frac{1-\varepsilon_1}{\varepsilon_1} \left(-\left.\frac{\partial \theta}{\partial Y}\right|_{Y=0^+} \right) + N_{rad}\theta_{w1}^4(Z) \right\}$$

$$*\frac{1}{2}\left[1+Re^2(Z-Z')^2\right]^{(-3/2)} Re\,dZ' = \frac{1-\varepsilon_2}{\varepsilon_2}\left[\left.\frac{\partial \theta_f}{\partial Y}\right|_{Y=1^-} -\right.$$

$$N_{rad}\,\theta_{w_2}^4(Z) - \left.\frac{\partial \theta_f}{\partial Y}\right|_{Y=1^-} \qquad (8)$$

When surface radiation is absent (i.e., $\varepsilon = 0$), equations (6) and (7) are reduced to:

$$\left.\frac{\partial \theta_f}{\partial Y}\right|_{Y=0} = 0 \qquad (9)$$

$$KR_{s_1-f} \left.\frac{\partial \theta_s}{\partial Y}\right|_{Y=1^+} = \left.\frac{\partial \theta_f}{\partial Y}\right|_{Y=1^-} \qquad (10)$$

Dimensionless boundary conditions must be defined.

At the channel entrance (Z = 0 and 0 < Y < 1):

$U = 1$, $V = P = 0$, and $\theta = \theta_\infty$ (11a)

At the first wall of the channel (Z > 0 and Y = 0):

$U = V = 0$ (11b)

At the second wall of the channel (Z > 0 and Y = 1): $U = V = 0$ (11c)

At the solid-solid interface of the solar cell assembly, for Z > 0, $Y = Y_{m_{(i)-(i+1)}}$, and i = 1 or 2:

$$\left.\frac{\partial \theta_s}{\partial Y}\right|_{Y=Y^-_{m_{(i)-(i+1)}}} = kR_{m_{(i+1)-(i)}} \left.\frac{\partial \theta_s}{\partial Y}\right|_{Y=Y^+_{m_{(i)-(i+1)}}}$$

For $Y = Y_{m_{(i)-(i+1)}}$, $0 < Z < Z_c$ or $(Z_c + L_c) < Z < L$, and i = 3 or 4:

$$\left.\frac{\partial \theta_s}{\partial Y}\right|_{Y=Y^-_{m_{(i)-(i+1)}}} = kR_{m_{(i+1)-(i)}} \left.\frac{\partial \theta_s}{\partial Y}\right|_{Y=Y^+_{m_{(i)-(i+1)}}} + \frac{(1-\eta)\,\alpha_{m_i}\,(1-\alpha_{m_8}-\alpha_{m_7})\,\bar{I}(Z)}{KR_{m_i-f}}$$

For $Y = Y_{m_{5-7}}$ and $0 < Z < Z_c$ or $(Z_c + L_c) < Z < L$:

$$\left.\frac{\partial \theta_s}{\partial Y}\right|_{Y=Y^-_{m_{5-7}}} = kR_{m_{7-5}} \left.\frac{\partial \theta_s}{\partial Y}\right|_{Y=Y^+_{m_{5-7}}} + \frac{(1-\eta)\,\alpha_{m_5}\,(1-\alpha_{m_8}-\alpha_{m_7})\,\bar{I}(Z)}{KR_{m_5-f}}$$

$Y=1^+$

For $Y = Y_{m_{(i)-(i+1)}}$, $Z_c \le Z \le (Z_c + L_c)$, and i = 3, 4, or 5:

$$\left.\frac{\partial \theta}{\partial Y}\right|_{Y=Y^-_{m_{(i)-(i+1)}}} = kR_{m_{(i+1)-(i)}} \left.\frac{\partial \theta}{\partial Y}\right|_{Y=Y^+_{m_{(i)-(i+1)}}}$$

For $Y = Y_{m_{6-7}}$ and $Z_c \le Z \le (Z_c + L_c)$:

$$\left.\frac{\partial\theta}{\partial Y}\right|_{Y=Y^-_{m_{6-7}}} = kR_{m_{7-6}} \left.\frac{\partial\theta}{\partial Y}\right|_{Y=Y^+_{m_{6-7}}} + \frac{\alpha_{m_6}(1-\alpha_{m_8}-\alpha_{m_7})\,\bar{I}(Z)}{kR_{m_6-f}}$$

For $Z > 0$ and $Y = Y_{m_{7-8}}$:

$$\left.\frac{\partial\theta}{\partial Y}\right|_{Y=Y^-_{m_{7-8}}} = kR_{m_{8-7}} \left.\frac{\partial\theta}{\partial Y}\right|_{Y=Y^+_{m_{7-8}}} + \frac{\alpha_{m_7}(1-\alpha_{m_8})\,\bar{I}(Z)}{kR_{m_7-f}}$$

For $Z > 0$ and $Y = Y_{m_8}$:

$$\left.\frac{\partial\theta}{\partial Y}\right|_{Y=Y_{m_8}} = \frac{\alpha_{m_8}\,\bar{I}(Z)}{kR_{m_8-f}}$$

In each case, $kR_{m_{(i+1)-i}} = \frac{k_{m_{i+1}}}{k_{m_i}}$ and $kR_{m_i-f} = \frac{k_{m_i}}{k_f}$

3. Method of Solution

The conjugate convection equations (continuity, momentum, and energy) are solved using a finite difference numerical marching technique while the two radiation constraint equations are solved iteratively using the Gauss-Seidel method. As a first iteration, the continuity, momentum, and energy equations, subject to the boundary conditions (Equations 9-11), are solved assuming that surface radiation is absent. The obtained solution is then utilized to solve the radiation constraint equations to update the temperature. These updated temperatures are used as new boundary conditions to resolve the convection equations. These procedures are repeated until convergence is achieved. Details of this method of solution and validation of the code can be found elsewhere (Al-Amri, 2008; Al-Amri and El-Shaarawi, 2010).

4. Results and Discussion

Temperature distribution on a solar cell surface is influenced by parameters related to the optical system, such as concentration ratio (C), the degree of non-uniformity of the incident light (as described by the S), and parameters related to the cooling system, such as the Reynolds number (Re) and channel wall emissivity (ε). In this study, the effects of three parameters (S, ε, and C) on cell temperature were investigated. Figure 2 illustrates how the solar cell temperature varies with the axial distance from the channel entrance for both uniform and non-uniform incident light at three values of S (0.0005, 0.001, and 0.002). Results show that when distribution is uniform, the solar cell temperature increases until reaching its maximum value at the channel exit. This maximum is less than 75°C, indicating that the triple-junction solar cell can be operated with acceptable conversion efficiency. However, when the distribution is non-uniform, the temperature profile takes the shape of a Gaussian distribution, and the maximum temperature occurs where maximum illumination occurs on the cell surface. In this case, the maximum temperature is extremely elevated relative to that seen with uniform light distribution. The lower the S, the higher the maximum temperature. Figure 3 shows the temperature distribution on the solar cell surface for three values of

emissivity, highlighting a small noticeable drop in maximum solar cell temperature as emissivity increases while the balance of the cell surface is nearly unchanged. This means that the effect of surface radiation on temperature distribution is negligible at low values of C, the opposite of what is seen at higher values (Al-Amri and Mallick, 2014, 2013).

Figures 4 and 5 show, for S = 0.0005, z_0 = 0.5, Re = 500, and ε = 0.95, the variations in cell temperature with axial distance from the channel entrance at three values of C and for non-uniform and uniform light profiles,

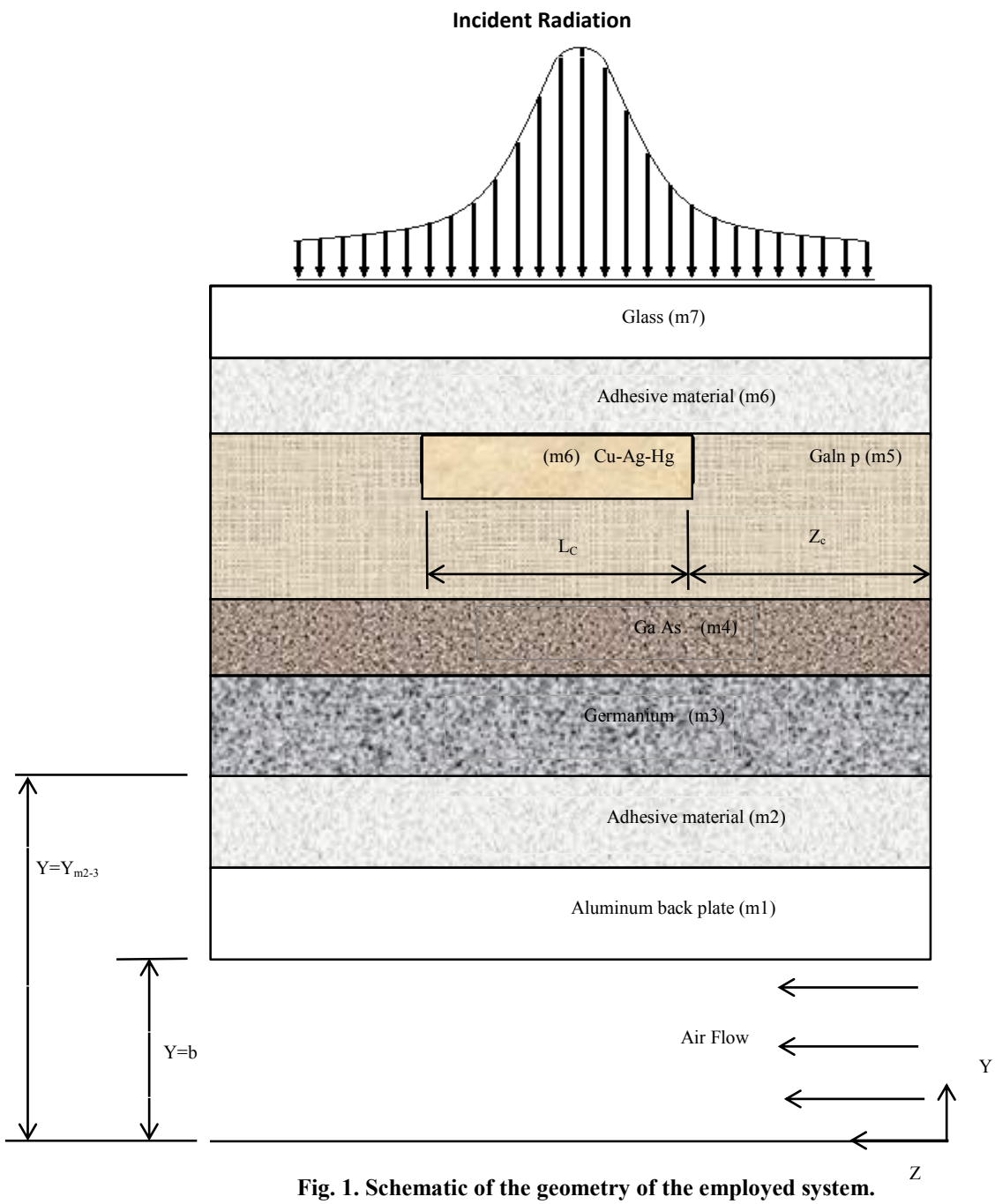

Fig. 1. Schematic of the geometry of the employed system.

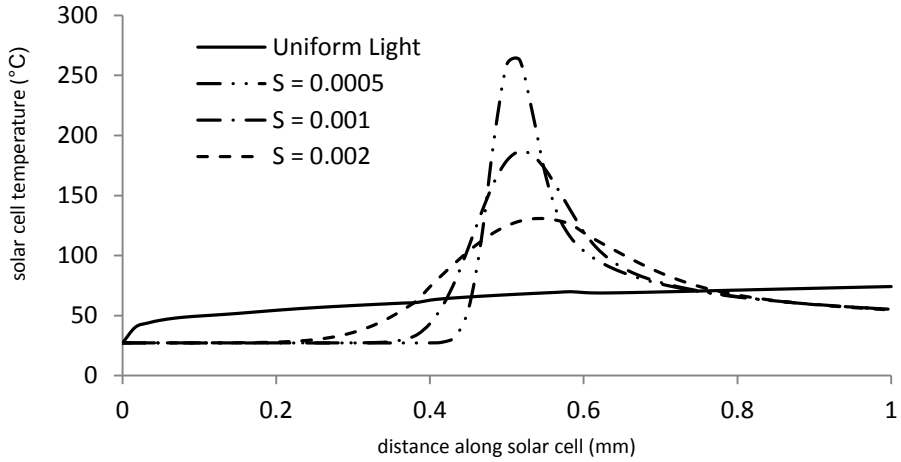

Fig. 2. Variations in solar cell temperature at various values of S when z_0 = 0.5, Re = 500, ε = 0.95, and C = 30.

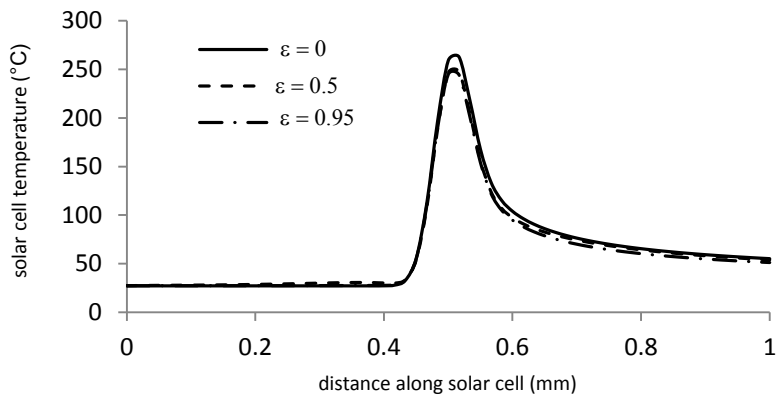

Fig. 3. Variations in solar cell temperature at various values of ε when S = 0.0005, z0 = 0.5, Re = 500, and C = 30.

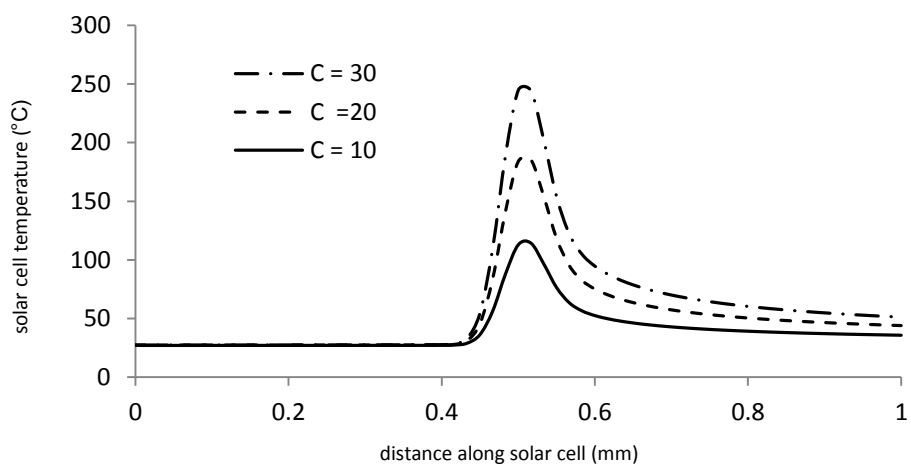

Fig. 4. Variations in solar cell temperature at various values of C when S = 0.0005, z0 = 0.5, Re = 500, and ε = 0.95.

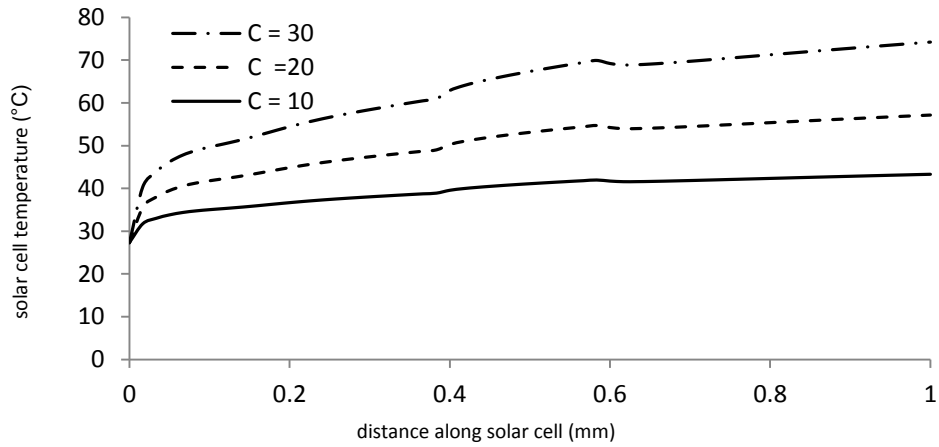

Fig. 5. Variations in solar cell temperature at various values of C when S = 0.0005, z0 = 0.5, Re = 500, and ε = 0.95.

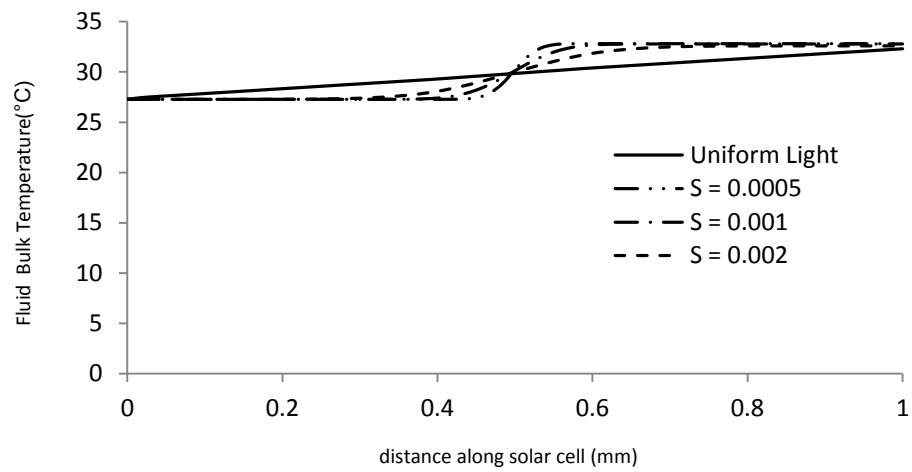

Fig. 6. Variations in fluid bulk temperature at various values of SD when z0 = 0.5, Re = 500, ε = 0.95, and C = 30.

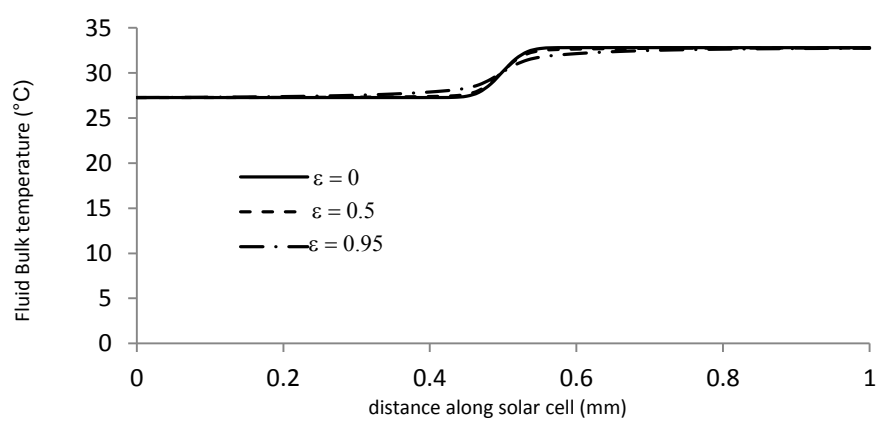

Fig. 7. Variations in fluid bulk temperature at various values of ε, when SD = 0.0005, z0 = 0.5, Re = 500, and C = 30.

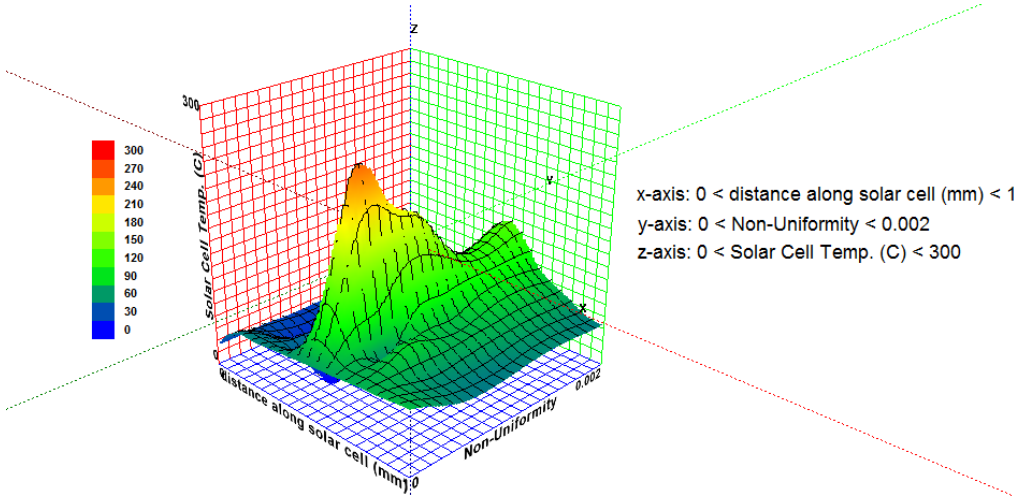

Fig. 8. 3-D Plot of Solar Cell Temperature as a Non-Linear Function of S along the length of solar cell.

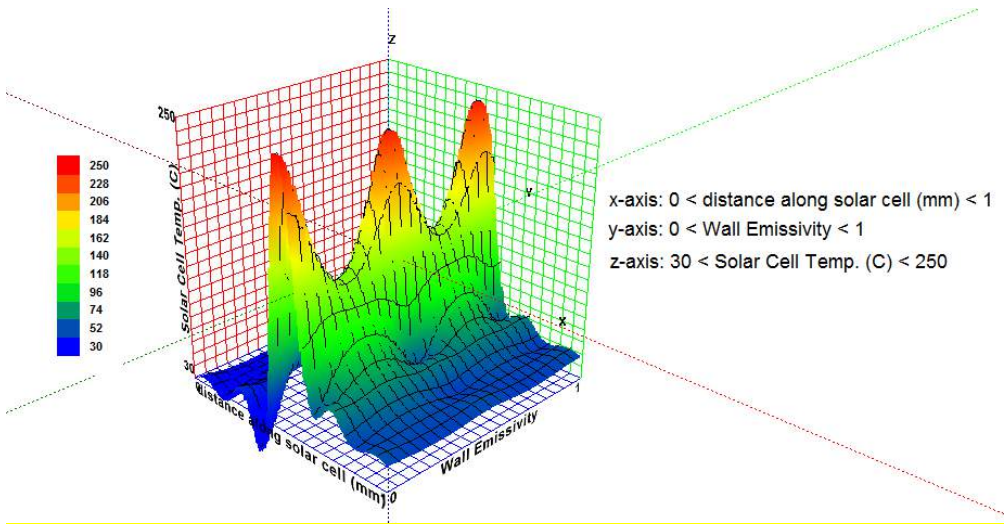

Fig. 9. 3-D Plot of Solar Cell Temperature as a Non-Linear Function of ε along the length of solar cell.

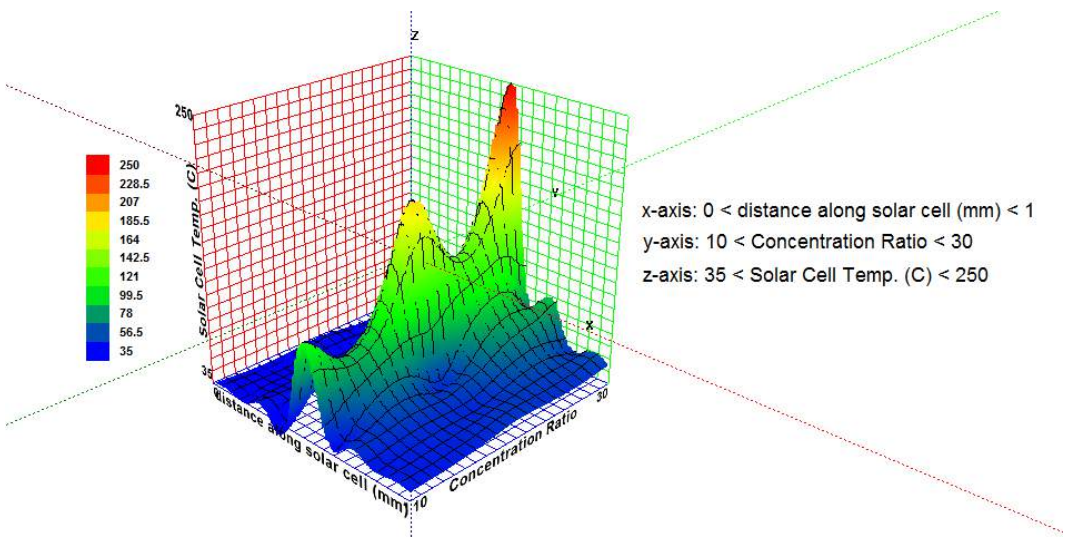

Fig. 10. 3-D Plot of Solar Cell Temperature as a Non-Linear Function of C along the length of solar cell.

respectively. It is obvious from the figures that maximum temperature increases significantly with C. Specifically, as C increased from 10 to 30 (i.e., by 200%) the maximum solar cell temperature increased by approximately 114% and 72% under non-uniform and uniform light, respectively. In addition, when the light distribution is non-uniform (Figure 5), the maximum temperature was above 100°C even when the concentration ratio was as low as 10, indicating that under non-uniform light distribution, a conventional plain channel is not appropriate for cooling the cell, even at low values of C.

Figure 6 shows the variation of fluid bulk temperature with the axial distance from the duct entrance under various incident illumination profiles. Results reveal that the shape of the incident light visibly affects the fluid bulk temperature profile inside the channel. However, the effect of the incident radiation profile on the fluid bulk temperature at the duct exit is insignificant. Figure 7 illustrates the emissivity effect of the two duct walls on the fluid bulk temperature. Surface radiation was found to have an insignificant effect on the fluid bulk temperature; therefore, it can be neglected. The effect of junction hotspot and temperature rise as a Non-Linear Function of the Three Parameters (S, ε, C) are shown in 3-D Plots given by figures 8, 9 & 10 respectively

5. Conclusions

When this numerical heat transfer model is used to simulate the temperature distribution on a concentrated solar cell under non-uniform incident radiation at low values of C, non-uniformity strongly alters the temperature distribution in the solar cell, causing hot spots in some regions. Maximum solar cell temperature increases as SD or C increases. However, surface radiation exchange inside the channel has only a slight effect on the solar cell temperature. In addition, plain channel cooling is inadequate for cooling the solar cell, even at low values of C. Although in the current study, the non-uniformity of the incident radiation was assumed to be normally distributed however, in practice, it is possible to have Biased Distribution Model which could be positively or negatively skewed due to varying shadowing/cloudy conditions. Still the results of the current study will be valid while the temperature distribution and location of hot spots would be shifted based on the skewness of the illumination distribution model.

References

Baig, H, Heasman, K. C., Mallick, T. K., 2012. Non-uniform Illumination in Concentrating Solar Cells, Renewable Sustainable Energy Reviews 16, pp 5890-5909.

Franklin, E., Conventry, J., 2003. "Effect of highly non-uniform illumination distribution on electrical performance of solar cell," Proceedings of Solar, Australian and New Zealand Solar Energy Society.

Conventry, J., Franklin, E., Blakers, A., 2002.

"Thermal and electrical performance of a concentrating PV/thermal collectors: Result from ANU CHAPS collector," 40th Conference of the Australia and New Zealand Solar Energy Society, Newcastle,.

Domenech-Garret, J-L., 2011. Cell Behavior Under Different Non-uniform Temperature and Radiation Combined Profiles Using a Two Dimensional Finite Element Model, Solar Energy 85, pp 256-265.

Chemisana, D., Rosell, J., 2011. Electrical performance increase of concentrator solar cells under Gaussian temperature profiles, Progress in Photovoltaics: Research and Applications.

Al-Amri, F., Mallick, T., 2014. Effects of Non-uniform Incident Illumination on the Thermal Performance of a Concentrating Triple Junction Solar Cell, International Journal of Photoenergy, Article ID 642819.

Xing, Y., Zhang, K., Zhao, J., Han, P., 2016. Thermal and Electrical Performance Analysis of Silica Vertical Multi-Junction Solar Cell under Non-uniform Illumination, Renewable Energy, 90, pp 77-82.

Al-Amri, F., Mallick, T. K., 2013. Alleviating Operating Temperature of Concentration Solar Cell by Air Active Cooling and Surface Radiation, Applied Thermal Engineering, 59, pp 348-354.

Al-Amri, F., 2008. "Effect of surface radiation on internal flows with non-isothermal boundary conditions," PhD Dissertation, King Fahd University of Petroleum & Minerals, Dhahran, Saudi Arabia.

Al-Amri, F. G., El-Shaarawi, M. A. I., 2010. Combined Forced Convection and Surface Radiation Between Two Parallel Plates," International Journal of Numerical Methods for Heat and FluidFlow, 20, pp 218–239.

Grubisic-Cabo, F. Nizetic, S. Marco, T., 2016. Photovoltaic Panels: A Review of the Cooling Techniques, Transactions of Famena XL- Special Issue 1. Pp 63-74.

Kumar, R., Rosen, M.A., 2011. A critical review of photovoltaic-thermal solar collectors for air heating, Applied Energy, 88, pp 3603-3614.

Nomenclature

b channel width, m

C concentration ratio

Gr^* modified Grashof number, $\frac{g\beta q_{avg} b^4}{\upsilon^2 K_f}$

I intensity of incident light, W/m^2

k thermal conductivity, $W/m \cdot K$

ℓ channel length, m

L dimensionless plate length, $\frac{\ell}{b\,Re}$

p pressure of fluid at any cross section, N/m^2

p' pressure defect at any cross section, p- p_s, N/m^2

p_s hydrostatic pressure, $-\rho_\infty gz$, N/m^2

p_∞ pressure of fluid at the channel entrance, N/m^2

P dimensionless pressure at any cross section, $\frac{p'-p_\infty}{\rho_\infty u_\infty^2}$

N_{rad} radiation number, $\sigma q_{avg}^3 b^4 / k_f^4$

q_{avg} average input heat flux, $(1-\eta)\, I_{avg}$, W/m^2

Re Reynolds number, $\frac{u_o b}{\upsilon}$

t solar cell assembly thickness, m

T temperature at any point, K

T_∞ inlet temperature, K

SD standard deviation

u_∞ entrance axial velocity, m/s

u longitudinal velocity component at any point, m/s

U dimensionless longitudinal velocity, u/ u_∞

v transverse velocity component at any point, m/s

V dimensionless transverse velocity, b * v / υ

y horizontal coordinate, m

Y dimensionless horizontal coordinate, y / b

z vertical coordinate, m

z_0 position of the maximum incident light, m

Z dimensionless vertical coordinate, z / (b * Re)

Greek Symbols

υ kinematic fluid viscosity

ρ fluid density, kg/m^3

μ dynamic fluid viscosity, $kg/m \cdot s$

α absorptivity

η efficiency of the solar cell

θ dimensionless temperature at any point $\left[\frac{k_f T}{q_{avg} b}\right]$

θ_∞ dimensionless inlet temperature at any point $\left[\frac{k_f T_\infty}{q_{avg} b}\right]$

ε wall emissivity

σ Stefan Boltzman constant, $5.67*10^{-8}$ W/m^2 k^4

Subscripts

c Cu-Ag-Hg front contact

e exit

f fluid

m material

s solid

w wall of the channel

∞ ambient or inlet

1 duct wall at Y = 0

2 duct wall at Y = 1